



ARCHIVIO ISTITUZIONALE DELLA RICERCA

Alma Mater Studiorum Università di Bologna Archivio istituzionale della ricerca

Synchrotron-based far-infrared spectroscopy of HC₃N: Extended ro-vibrational analysis and new line list up to 3360 cm⁻¹

This is the final peer-reviewed author's accepted manuscript (postprint) of the following publication:

Published Version:

Synchrotron-based far-infrared spectroscopy of HC₃N: Extended ro-vibrational analysis and new line list up to 3360 cm⁻¹ / Tamassia F.; Bizzocchi L.; Melosso M.; Martin-Drumel M.-A.; Piralì O.; Pietropoli Charmet A.; Cane' E.; Dore L.; Gordon I.E.; Guillemin J.-C.; Giuliano B.M.; Caselli P.; Alessandrini S.; Barone V.; Puzzarini C.. - In: JOURNAL OF QUANTITATIVE SPECTROSCOPY & RADIATIVE TRANSFER. - ISSN 0022-4073. - STAMPA. - 279:(2022), pp. 108044.108044-1-108044.108044-13. [10.1016/j.jqsrt.2021.108044]

This version is available at: <https://hdl.handle.net/11585/872019> since: 2022-11-23

Published:

DOI: <http://doi.org/10.1016/j.jqsrt.2021.108044>

Terms of use:

Some rights reserved. The terms and conditions for the reuse of this version of the manuscript are specified in the publishing policy. For all terms of use and more information see the publisher's website.

(Article begins on next page)

This item was downloaded from IRIS Università di Bologna (<https://cris.unibo.it/>).
When citing, please refer to the published version.

This is the final peer-reviewed accepted manuscript of:

Tamassia, F., Bizzocchi, L., Melosso, M., Martin-Drumel, M.-A., Pirali, O., Pietropoli Charmet, A., Canè, E., Dore, L., Gordon, I.E., Guillemin, J.-C., Giuliano, B.M., Caselli, P., Alessandrini, S., Barone, V., Puzzarini, C., 2022. Synchrotron-based far-infrared spectroscopy of HC3N: Extended ro-vibrational analysis and new line list up to 3360 cm⁻¹. *Journal of Quantitative Spectroscopy and Radiative Transfer* 279, 108044.

The final published version is available online at:
<https://doi.org/10.1016/j.jqsrt.2021.108044>

Rights / License:

The terms and conditions for the reuse of this version of the manuscript are specified in the publishing policy. For all terms of use and more information see the publisher's website.

This item was downloaded from IRIS Università di Bologna (<https://cris.unibo.it/>)

When citing, please refer to the published version.

Synchrotron-based far-infrared spectroscopy of HC₃N: extended ro-vibrational analysis and new line list up to 3360 cm⁻¹

Filippo Tamassia^{a,*}, Luca Bizzocchi^{b,c,*}, Mattia Melosso^{c,*}, Marie-Aline Martin-Drumel^d, Olivier Pirali^{d,e}, Andrea Pietropoli Charmet^f, Elisabetta Canè^a, Luca Dore^c, Iouli E. Gordon^g, Jean-Claude Guillemin^h, Barbara M. Giulianoⁱ, Paola Caselliⁱ, Silvia Alessandrini^{b,c}, Vincenzo Barone^b, Cristina Puzzarini^c

^a*Dipartimento di Chimica Industriale “Toso Montanari”, Università di Bologna, Viale del Risorgimento 4, 40136 Bologna, Italy*

^b*Scuola Normale Superiore, Piazza dei Cavalieri 7, 56126 Pisa, Italy*

^c*Dipartimento di Chimica “Giacomo Ciamician”, Università di Bologna, Via F. Selmi 2, 40126 Bologna, Italy*

^d*Université Paris-Saclay, CNRS, Institut des Sciences Moléculaires d’Orsay, 91405 Orsay, France*

^e*SOLEIL Synchrotron, AILES beamline, l’Orme des Merisiers, Saint-Aubin, 91190 Gif-sur-Yvette, France*

^f*Dipartimento di Scienze Molecolari e Nanosistemi, Università Ca’ Foscari Venezia, Via Torino 155, 30172 Mestre, Italy*

^g*Harvard-Smithsonian Center for Astrophysics, Atomic and Molecular Physics Division, Cambridge, MA, USA*

^h*Université de Rennes, Ecole Nationale Supérieure de Chimie de Rennes, CNRS, ISCR-UMR6226, 35000 Rennes, France*

ⁱ*Center for Astrochemical Studies, Max Planck Institut für extraterrestrische Physik Gießenbachstraße 1, 85748 Garching bei München, Germany*

Abstract

The far-infrared spectrum of HC₃N has been recorded at high resolution between 70 and 500 cm⁻¹ using synchrotron radiation. Four prominent features, i.e., ν_7 , $\nu_6 - \nu_7$, $\nu_4 - \nu_6$, and $2\nu_7$ have been identified in the spectrum together with many associated hot bands. In addition, rotational transitions for the interacting $v_4 = v_7 = 1$, $(v_6 = 2, v_7 = 1)$, $(v_5 = 1, v_7 = 2)$, and $v_7 = 5$ vibrationally excited states have been recorded in the millimeter/submillimeter region. The newly assigned transitions, together with those reported previously, form a comprehensive data set including about 17 000 transitions, which involves almost all the vibrational states of HC₃N lying below 1300 cm⁻¹ plus some excited states with energies between 2075 and 3550 cm⁻¹. These data have been fitted to an effective Hamiltonian which takes into account rotational and vibrational l -type resonance effects, together with a number of anharmonic interaction terms. On average, all the analysed data are reproduced within the experimental accuracy. About 90 000 rotational and ro-vibrational transition frequencies have been computed on the basis of the spectroscopic constants obtained from the global fit in order to support data interpretation and astronomical searches in the interstellar medium and planetary atmospheres. Part of these data is included in the 2020 release of the HITRAN database.

Keywords: Cyanoacetylene, Interstellar matter, Molecular spectroscopy, Spectroscopic database, Energy levels, Ro-vibrational spectra

1. Introduction

Cyanoacetylene (HC₃N) is a simple linear molecule of great astrochemical interest. Its relevance has been demonstrated by the huge amount of observational studies carried out in the past decades, which revealed HC₃N to be an ubiquitous interstellar species, detected in molecular clouds [1], comets [2], nearby galaxies [3], and planetary atmospheres [4]. Recent observations have pointed out its importance as tracer

*Supplementary material available.

*Corresponding authors

Email addresses: filippo.tamassia@unibo.it (Filippo Tamassia), luca.bizzocchi@unibo.it (Luca Bizzocchi), mattia.melosso2@unibo.it (Mattia Melosso)

6 of the chemical evolution of molecular clouds [5] or — through the DC₃N isotopologue — as proxy of the
7 deuteration level prior to the formation of dense gas in star-forming regions [6]. Moreover, cyanoacetylene
8 emission has been used to unravel the seasonal changes and atmospheric dynamics of the largest Saturn’s
9 moon Titan [7] and is predicted to be detectable in Super-Earth atmospheres by upcoming James Webb
10 Telescope observations [8]. Interestingly, vibrationally excited HC₃N has been also observed in Space. For
11 example, pure rotational transitions in vibrational states up to 1100 cm⁻¹ have been detected in the proto-
12 planetary nebula CRL 618 [9] (see also a more recent account for NGC 1068 [10]).

13 The laboratory investigation of the rotational and ro-vibrational spectra of HC₃N, which is essential for
14 guiding astronomical searches of this species, has been pushed forward for 70 years. To date, the most
15 comprehensive spectroscopic analysis of cyanoacetylene has been reported in our previous study (Ref. [11],
16 hereafter Paper I), where a comprehensive list of references for laboratory detections and observations
17 in Space is also provided. In Paper I, the HC₃N infrared spectrum has been recorded between 450 and
18 1100 cm⁻¹ and analyzed focusing on all the vibrational states with energy below 1000 cm⁻¹, for which a
19 sizable number of rotational transitions were also observed. The global analysis performed in Paper I allowed
20 to derive a consistent set of spectroscopic rotational and vibrational parameters for all the twelve vibrational
21 states investigated, and includes the accurate modelling of two networks of anharmonic resonances which
22 substantially perturb the spectra. Yet, the dataset of Paper I did not include any ro-vibrational transitions
23 located in the far-infrared (FIR, here below 450 cm⁻¹) portion of the spectrum as well as none of the
24 stretching bands, observed roughly between 2000 and 3400 cm⁻¹. While no spectrum was reported in the
25 literature for the FIR region, some data were available for the stretching modes. In particular, after the first
26 medium resolution (0.025–0.050 cm⁻¹) study of the 1800–6500 cm⁻¹ region [12], higher-resolution spectra of
27 the ν_1 [13], ν_2 [14], ν_3 [15], and some of their hot-bands [13, 16] were reported.

28 Theoretical calculations involving fundamental, combination, overtone, and hot bands between 200 and
29 4800 cm⁻¹ have been recently published [17], as well as estimates for the infrared fundamental intensities
30 [18]. Previously, various theoretical works on the force field, dipole functions, and molecular structure were
31 also presented [19, 20, 21, 22].

32 However, the data available in the literature for the stretching modes indicated that the experimental
33 dataset could be extended and recorded at a higher, homogeneous resolution. Therefore, we recently re-
34 investigated the ν_1 , ν_2 , and ν_3 bands and their associated hot bands $\nu_1 + \nu_7 - \nu_7$, $\nu_2 + \nu_7 - \nu_7$, $\nu_3 + \nu_7 - \nu_7$
35 by Fourier transform infrared (FTIR) spectroscopy [23] at an instrumental resolution of 0.004 cm⁻¹.

36 Here, to fill the lack of HC₃N data in the FIR window, we undertake for the first time a detailed analysis
37 of the region below 450 cm⁻¹, by recording FTIR spectra at the SOLEIL synchrotron facility as recently
38 done for DC₃N [24]. In addition, a new network of anharmonic resonances involving vibrational states with
39 energies around 1200 cm⁻¹ is identified and modelled on the basis of (i) spectra recorded but not analyzed
40 in Paper I and (ii) new rotational measurements performed in this work. The ultimate goal of the present
41 paper is to achieve an improved fit of all the HC₃N data in order to attain a very accurate and extended
42 set of ro-vibrational constants and, consequently, a comprehensive line list to be used for astronomical
43 observations of cyanoacetylene at different wavelengths.

44 2. Experiments

45 The new rotational and ro-vibrational spectra described in this work have been recorded in three labora-
46 tories: the FIR spectrum has been observed at the SOLEIL synchrotron facility, while the millimeter (mm)
47 and submillimeter (submm) spectra have been measured in Bologna and in Garching. The preparation of
48 the sample used for the measurements has been described in Paper I.

49 The FIR spectrum of HC₃N has been recorded at the AILES beamline of SOLEIL using a Bruker IFS
50 125 FT interferometer [25] associated to a White-type multi-pass absorption cell whose optics were adjusted
51 to obtain 150 m optical path length [26, 27]. The synchrotron radiation extracted by the AILES beamline
52 was used as the FIR source of continuum for the FT interferometer. The interferometer was equipped with a
53 6 μ m Mylar-composite beamsplitter and a 4 K cooled Si-bolometer and was isolated from the interferometer
54 by two 50 μ m-thick polypropylene windows. The optics compartment was continuously evacuated to 0.01 Pa

55 in order to limit the absorption of atmospheric water. Vapor of HC_3N was injected into the absorption cell
 56 at 1.5, 3.5 and 28.6 Pa pressure. The spectrum covers the range $70\text{--}500\text{ cm}^{-1}$ and was recorded at different
 57 pressures and with a different number of scans: 400 scans at 1.5 and 28.6 Pa, 360 scans at 1.5 Pa. The
 58 instrumental resolution was 0.001 cm^{-1} . No apodization function was applied to the interferogram. The
 59 wavenumber-axis of the spectra has been calibrated using residual water absorption lines, whose reference
 60 wavenumbers were taken from [28] and [29]. Based on the dispersion after calibration, line frequencies are
 61 expected to be as accurate as 0.0001 cm^{-1} .

62 A number of new mm-wave spectra have been recorded at the Center for Astrochemical Studies in the
 63 $80\text{--}175\text{ GHz}$ frequency interval using the CASAC spectrometer already described in details elsewhere [30].
 64 Additional measurements in selected frequency intervals between 260 and 450 GHz have been performed in
 65 Bologna using a frequency-modulation (FM) mm-wave spectrometer, whose description has been reported in
 66 Refs. [31, 32]. In both these latter laboratories, the spectra were recorded at room temperature, using static
 67 samples at a pressure of $0.3\text{--}1.0\text{ Pa}$. The transition frequencies were recovered from a line-shape analysis
 68 of the spectral profile [33] and their accuracy, estimated by repeated measurements and depending on the
 69 attained S/N, is in the $5\text{--}30\text{ kHz}$ range.

70 This work also reports on the analysis of some vibrational bands observed in the spectra previously
 71 recorded in Bologna using a Bomem DA3.002 Fourier-transform spectrometer [11, 23] and not included in
 72 Paper I. For further details about the recording conditions, the readers are referred to Bizzocchi et al. [11]
 73 and Jiang et al. [23] for the regions $450\text{--}1050\text{ cm}^{-1}$ and $1900\text{--}3400\text{ cm}^{-1}$, respectively.

74 3. Observed spectra

75 Cyanoacetylene is a linear molecule with seven vibrational normal modes: four stretching modes ($\nu_1, \nu_2,$
 76 ν_3, ν_4 ; Σ symmetry) and three doubly degenerate bending modes (ν_5, ν_6, ν_7 ; Π symmetry). All of them are
 77 infrared active.

78 A portion of the vibrational energy manifold of HC_3N is schematically shown in Figure 1. All the levels
 79 involved in the present analysis are plotted in solid black lines, while the appearance of the infrared spectra
 80 is depicted sideways on the left. Our study includes all the vibrational fundamentals as well as all the excited
 81 levels below 1300 cm^{-1} with the only exception of the $v_5 = v_6 = 1$ state. This combination mode, together
 82 with the $v_5 = 2$ overtone state, is involved in a complex network of anharmonic resonances and will be the
 83 object of a future investigation. In total, 24 bands have been identified and analysed in this work. They are
 84 summarised in Table 1.

85 3.1. The $190\text{--}450\text{ cm}^{-1}$ region

86 The far infrared region shows many bands starting from 200 cm^{-1} . A recording of this spectral range
 87 is shown in Figure 2, together with a stick-spectrum simulation to allow for the identification of the most
 88 prominent features. The fundamental ν_7 , around 220 cm^{-1} , has been observed for the first time in this
 89 work, although a precise determination of its vibrational energy had been already achieved indirectly in
 90 Paper I. Nevertheless, the resolution and sensitivity of the FIR spectrum recorded at the SOLEIL facility
 91 has confirmed and improved both precision and accuracy of the spectroscopic constants related to the ν_7
 92 vibrational mode.

93 The excitation of the ν_7 mode gives rise to different manifolds for increasing values of the vibrational
 94 angular quantum number l , labelled as $\Sigma, \Pi, \Delta, \Phi, \Gamma, \text{H}$ for $l = 0, 1, 2, 3, 4, 5$, respectively. All the possible
 95 allowed transitions between those energy levels, according to the selection rule $\Delta l = \pm 1$, have been identified,
 96 with the exception of the $5\nu_7 - 4\nu_7$ hot-band, for which only the $\text{H} \leftarrow \Gamma$ component has been assigned. In the
 97 same portion of the spectrum, almost all the sub-bands of the $\nu_6 + \nu_7 - \nu_6, \nu_5 + \nu_7 - \nu_5$, and $\nu_6 + 2\nu_7 - \nu_6 - \nu_7$
 98 have been also assigned, which show very weak, if not barely detectable, Q -branches.

99 At higher wavenumbers, the $\nu_6 - \nu_7$ ($\sim 277\text{ cm}^{-1}$) and $\nu_4 - \nu_6$ ($\sim 363\text{ cm}^{-1}$) difference bands, and the
 100 $2\nu_7$ overtone ($\sim 443\text{ cm}^{-1}$) do have notable intensity as well. For all these transitions, eight associated hot
 101 bands have been identified and analysed. Apart from $\nu_4 - \nu_6$ and its $\nu_4 + \nu_7 - \nu_6 - \nu_7$ hot band, which
 102 have a prominent Q -branch ($\Delta l = \pm 1$), all these features show a parallel structure with strong P - and R -
 103 branches and no Q -branch.

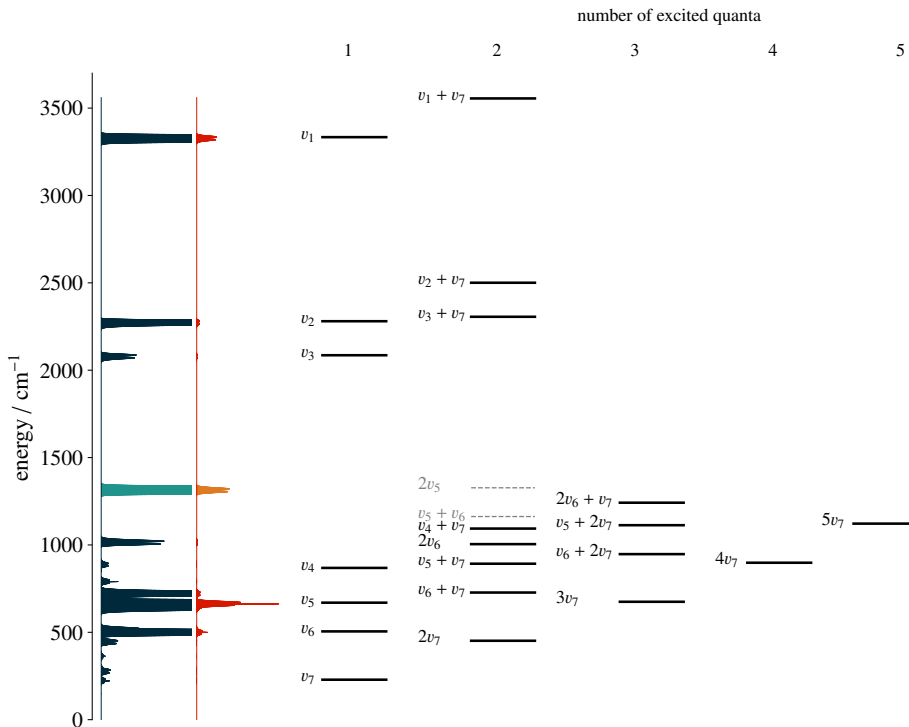


Figure 1: Schematic representation of the vibrational energy manifold of HC_3N (complete below 1300 cm^{-1}). The states investigated in this work are drawn in black solid lines. Grey dashed lines indicate the levels not considered in the present analysis. On the left, the appearance of the vibrational spectrum of HC_3N is depicted sideways adopting two different normalisation factors. The intensity of the red trace is adjusted to show the prominent ν_1 , ν_5 , and ν_6 bands, whereas the dark blue spectrum is expanded 50 times in order to show the weaker bands. Note that the $2\nu_5$ overtone (labelled with paler colour in the plots) is the only major spectral feature not covered by the present analysis (see text).

104 3.2. The $450\text{--}1050\text{ cm}^{-1}$ region

105 This spectral window, dominated by the very strong ν_5 fundamental and the strong ν_6 and $\nu_6 + \nu_7$ bands,
 106 has been discussed in detail in Paper I. However, some new features have been identified and analysed in
 107 this work. They are the ν_7 -associated hot-bands of the ν_4 and $2\nu_6$ bands, the ν_6 -associated hot-band of the
 108 $\nu_6 + \nu_7$ combination, the $2\nu_7$ -associated hot-band of the ν_5 vibration, plus the new $\nu_4 + \nu_7 - \nu_6$ difference
 109 band.

110 3.3. The $1900\text{--}3400\text{ cm}^{-1}$ region

111 As summarized in the introduction, this region had been studied in the past by several authors, who
 112 employed different spectroscopic techniques, such as tunable diode lasers and FTIR. The re-investigation
 113 of this region was motivated by the need to have a complete coverage at a homogeneous high-resolution of
 114 the three higher energy stretching bands ν_1 ($\sim 3327\text{ cm}^{-1}$), ν_2 ($\sim 2274\text{ cm}^{-1}$), and ν_3 ($\sim 2079\text{ cm}^{-1}$) and
 115 of their strongest associated hot bands. The analysis of these bands has been reported in a recent paper
 116 focused on DC_3N [23].

117 The fundamentals ν_1 , ν_2 , and ν_3 are all intense bands of $\Sigma - \Sigma$ symmetry, for which many P and R
 118 transitions could be assigned, up to $J = 110$ for ν_1 , $J = 105$ for ν_2 , and $J = 110$ for ν_3 . The identification
 119 of the first hot bands $\nu_1 + \nu_7(\text{II}) - \nu_7(\text{II})$, $\nu_2 + \nu_7(\text{II}) - \nu_7(\text{II})$, $\nu_3 + \nu_7(\text{II}) - \nu_7(\text{II})$ was rather straightforward

Table 1: Ro-vibrational bands of HC₃N recorded and analysed in this work.

Band	Sub-bands	Freq. range (cm ⁻¹)	J max	No. of lines	rms ^a ×10 ⁴ (cm ⁻¹)
ν_7	$\Pi - \Sigma^+$	194 - 257	106	304	0.4 (0.5)
$2\nu_7 - \nu_7$	$(\Sigma^+, \Delta) - \Pi$	196 - 253	99	654	0.6 (0.5)
$3\nu_7 - 2\nu_7$	$(\Pi, \Phi) - (\Sigma^+, \Delta)$	197 - 251	88	869	0.8 (0.75)
$4\nu_7 - 3\nu_7$	$(\Sigma^+, \Delta, \Gamma) - (\Pi, \Phi)$	199 - 249	86	858	1.2 (1.0)
$5\nu_7 - 4\nu_7$	H - Γ	209 - 240	51	115	1.3 (1.5)
$\nu_6 + \nu_7 - \nu_6$	$(\Sigma, \Delta) - \Pi$	201 - 247	81	479	1.3 (1.0)
$\nu_5 + \nu_7 - \nu_5$	$(\Sigma, \Delta) - \Pi$	202 - 248	76	405	1.2 (1.0)
$\nu_6 + 2\nu_7 - \nu_6 - \nu_7$	$(\Pi, \Phi) - (\Sigma^+, \Delta)$	205 - 247	71	266	0.2 (0.5)
$\nu_6 - \nu_7$	$\Pi - \Pi$	247 - 303	90	345	0.6 (0.75)
$\nu_6 + \nu_7 - 2\nu_7$	$(\Sigma^+, \Delta) - (\Sigma^+, \Delta)$	249 - 302	86	472	0.5 (0.75)
$2\nu_6 - \nu_6 - \nu_7$	$(\Sigma^+, \Delta) - (\Sigma^+, \Delta)$	248 - 316	89	439	1.0 (1.0)
$\nu_6 + 2\nu_7 - 3\nu_7$	$(\Pi, \Phi) - (\Pi, \Phi)$	247 - 303	91	837	1.4 (1.5)
$\nu_4 - \nu_6$	$\Sigma^+ - \Pi$	331 - 387	94	256	0.5 (0.5)
$\nu_4 + \nu_7 - \nu_6 - \nu_7$	$\Pi - (\Sigma, \Delta)$	342 - 385	72	564	1.0 (1.0)
$2\nu_7$	$\Sigma^+ - \Sigma^+$	422 - 468	88	152	0.8 (0.75)
$3\nu_7 - \nu_7$	$(\Pi, \Phi) - \Pi$	420 - 467	87	297	1.0 (1.0)
$4\nu_7 - 2\nu_7$	$(\Sigma^+, \Delta) - \Sigma^+, \Delta)$	420 - 443	83	420	1.2 (1.0)
$5\nu_7 - 3\nu_7$	$(\Pi, \Phi) - (\Pi, \Phi)$	419 - 462	77	379	1.7 (1.5)
$\nu_6 + 2\nu_7 - \nu_6$	$\Pi - \Pi$	426 - 467	68	180	2.0 (2.0)
$\nu_4 + \nu_7 - \nu_6$	$\Pi - \Pi$	566 - 610	73	267	2.0 (5.0)
$\nu_5 + 2\nu_7 - 2\nu_7$	$(\Pi, \Phi) - (\Sigma^+, \Delta)$	634 - 690	105	704	2.7 (4.0)
$2\nu_6 + \nu_7 - \nu_6$	$\Pi - \Pi$	702 - 756	81	346	5.5 (5.0)
$\nu_4 + \nu_7 - \nu_7$	$\Pi - \Pi$	847 - 881	55	87	8.8 (10)
$2\nu_6 + \nu_7 - \nu_7$	$\Pi - \Pi$	991 - 1039	79	227	6.6 (5.0)

^a Root mean square deviation of the global fit. The assumed experimental precision of each band is given in parentheses (see § 4.1).

 Table 2: Rotational transitions of HC₃N recorded in this work.

State	Freq. range (GHz)	J max	No. of lines	rms ^a (kHz)
$v_4 = v_7 = 1$	73 - 791	86	83	0.209
$v_6 = 2, v_7 = 1$	82 - 422	45	157	0.048
$v_5 = 1, v_7 = 2$	82 - 422	45	155	0.043
$v_7 = 5$	83 - 508	54	128	0.022
inter-state	376 - 424	45	10	0.038

^a Root mean square deviation of the global fit.

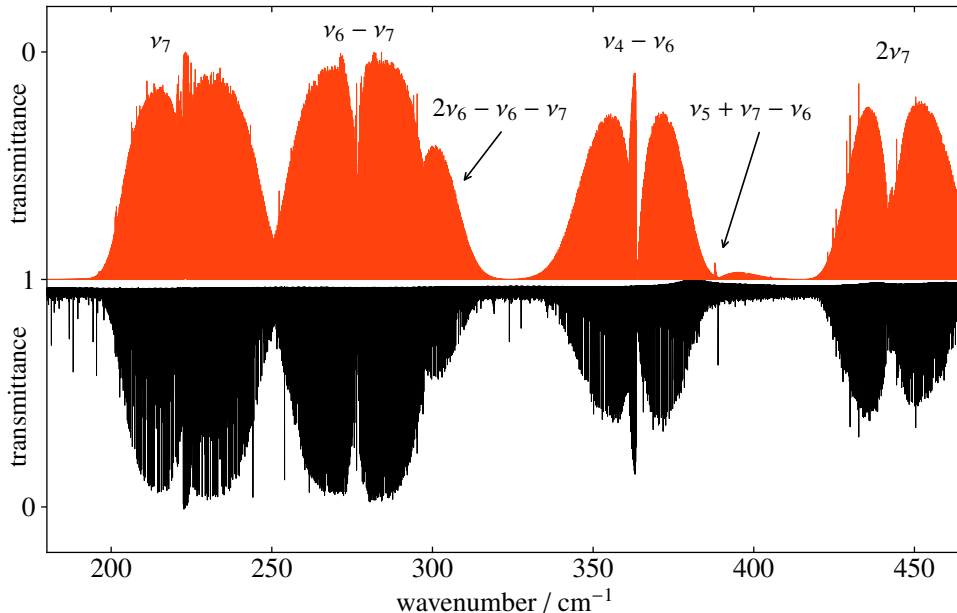


Figure 2: Recorded FIR spectrum from 180 to 465 cm^{-1} (black trace). Synthetic transmission spectrum (orange trace) was computed based on the line list presented in this work using HITRAN Application Programming Interface (HAPI) [34]. The simulated spectrum has been displayed as reversed transmittance for a better comparison with the experimental one. Lines belonging to H_2O were removed from the experimental spectrum. Experimental conditions: $T = 298 \text{ K}$, $P = 28.6 \text{ Pa}$, $L = 150 \text{ m}$, 400 scans, unapodized resolution 0.001 cm^{-1} .

120 and also for these bands many transitions could be assigned. The Q branches of the hot bands, although
 121 allowed by symmetry, were not detected. No evidence of strong perturbations has been found.

122 3.4. Rotational spectrum

123 The rotational spectrum of HC_3N has already been studied extensively in the ground and in many
 124 vibrationally excited states (see Paper I and references therein). In the context of the present investigation,
 125 we have recorded additional mm- and submm-wave data for a subset of vibrational states located between
 126 1050 and 1200 cm^{-1} : they are $\nu_4 = \nu_7 = 1$, $(\nu_6 = 2, \nu_7 = 1)$, $(\nu_5 = 1, \nu_7 = 2)$, and $\nu_7 = 5$. The new
 127 measurements have been performed in Bologna and Garching focusing on selected frequency windows in
 128 the 80–450 GHz interval (an example is given in Fig. 3). A particular attention has been devoted to the
 129 $J = 40 - 46$ region (340–420 GHz) where the lines belonging to the nearly-degenerate $(\nu_5 = 1, \nu_7 = 2)$
 130 and $\nu_7 = 5$ vibrational states show large deviations from their unperturbed positions owing to the avoided
 131 crossings between the various interacting sub-levels.

132 4. Analysis and Results

133 The computation of the ro-vibrational energy terms of HC_3N follows the procedure described in detail
 134 in Paper I. Briefly, the effective Hamiltonian is a sum of a ro-vibrational (\tilde{H}_{rv}) and a l -type interaction
 135 ($\tilde{H}_{l\text{-type}}$) contributions, plus a term (\tilde{H}_{res}) describing the accidental anharmonic resonances present in this
 136 molecule:

$$\tilde{H} = \tilde{H}_{\text{rv}} + \tilde{H}_{l\text{-type}} + \tilde{H}_{\text{res}}. \quad (1)$$

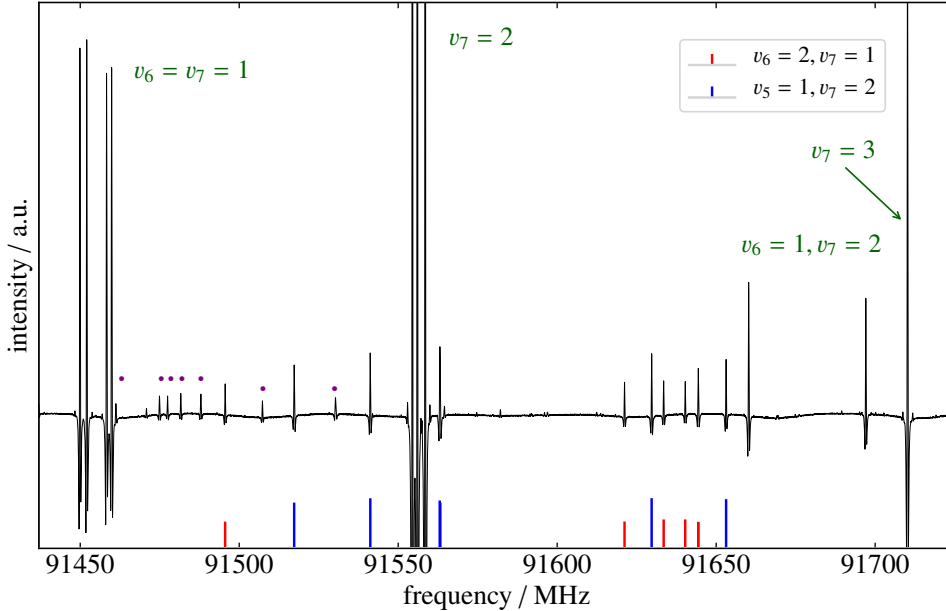


Figure 3: Excerpt of the $J = 10 \leftarrow 9$ transition of HC_3N in the region of multiple excited bending states. The stick spectrum indicates the position of the $(v_6 = 2, v_7 = 1)$ state (red) and $(v_5 = 1, v_7 = 2)$ (blue) combinations located at $1100\text{-}1200\text{ cm}^{-1}$. The green labels identify the strong components belonging to some lower-energy vibrationally excited states. The purple dots mark the lines of the $(v_5 = v_6 = v_7 = 1)$ three-bending combination states which have not been analysed in this study. Spectrum recorded with the CASAC spectrometer [30] using a scan speed of 1.2 MHz s^{-1} and $RC = 3\text{ ms}$.

137 \tilde{H}_{rv} is diagonal in all quantum numbers, whereas $\tilde{H}_{l\text{-type}}$ gives rise to several matrix elements off-diagonal
 138 in the l_t quantum numbers and according to the selection rules $\Delta k = 0, \pm 2, \pm 4$. \tilde{H}_{res} contains terms
 139 connecting the sub-blocks of the nearly-degenerate, interacting vibrational states. The complete expressions
 140 of the Hamiltonian is given in Paper I.

141 Below 1050 cm^{-1} two networks of anharmonic interactions have been identified: (i) $v_5 = 1 \sim v_7 = 3$
 142 around 660 cm^{-1} and (ii) $v_4 = 1 \sim v_5 = v_7 = 1 \sim v_6 = 2 \sim v_7 = 4$ centered at 880 cm^{-1} . Both resonance
 143 systems have been investigated and the corresponding interaction parameters determined from the global
 144 analysis. They are associated to the resonance Hamiltonian terms $H_{30}, H_{32}, H_{40}, H_{42}, H_{50}$, and H_{52} . Here,
 145 the Hamiltonian is labelled as \tilde{H}_{mn} , where m and n are the total degree of the vibrational and rotational
 146 operators, respectively. The same types of interaction take place if one quantum of vibrational energy is
 147 added to each energy level involved in the interactions. If the pair (i) is upscaled by adding one v_7 quantum,
 148 we obtain some terms of the resonance system (ii), whereas the same operation on (ii) generates a new
 149 network of interacting states located approximately at 1100 cm^{-1} : $v_4 = v_7 = 1 \sim (v_5 = 1, v_7 = 2) \sim (v_6 =$
 150 $2, v_7 = 1) \sim v_7 = 5$. This resonance system has been investigated thoroughly for the first time in this
 151 work. In addition to the \tilde{H}_{res} terms cited above, for this analysis **we considered further contributions**
 152 produced by the \tilde{H}_{32} transformed Hamiltonian:

$$\begin{aligned} & \left\langle v_4, v_5^{l_5}, v_6^{l_6}, v_7^{l_7}; J, k \left| \tilde{H}_{32} \right| v_4 + 1, (v_5 - 1)^{l_5 \pm 1}, v_6^{l_6}, (v_7 - 1)^{l_7 \pm 1}; J, k \pm 2 \right\rangle \\ & = \frac{\sqrt{2}}{2} C_{32} [(v_4 + 1)(v_5 \pm l_5)(v_7 \pm l_7)]^{1/2} \sqrt{f_{\pm 2}(J, k)}, \quad (2) \end{aligned}$$

153 where the k -dependent term of the matrix element is given by (see Eq. (3b) of Paper I for the general

154 formula):

$$f_{\pm 2}(J, k) = [J(J + 1) - k(k \pm 1)] [J(J + 1) - (k \pm 1)(k \pm 2)] . \quad (3)$$

155 This interaction has been considered in association with the classic cubic anharmonic resonance \tilde{H}_{30}
 156 involving the $(v_4 = v_7 = 1)$ and $(v_5 = 1, v_7 = 2)$ states and provides additional $\Delta k \pm 2$ couplings.

157 The ro-vibrational basis functions are chosen as product of one-/two-dimensional harmonic oscillator
 158 wave-functions and a rotational symmetric-top wave-function, $|v_s, v_5^{l_5}, v_6^{l_6}, v_7^{l_7}; J, k\rangle$, with $k = l_5 + l_6 + l_7$. In
 159 this notation v_s summarizes the stretching mode vibrational quantum numbers v_1, v_2, v_3 and v_4 . Symmetry-
 160 adapted basis functions are then obtained by the Wang-type linear combinations [35]:

$$\begin{aligned} & |v_s, v_5^{l_5}, v_6^{l_6}, v_7^{l_7}; J, k\rangle_{e/f} \\ &= \frac{1}{\sqrt{2}} \left\{ |v_s, v_5^{l_5}, v_6^{l_6}, v_7^{l_7}; J, k\rangle \pm (-1)^k |v_s, v_5^{-l_5}, v_6^{-l_6}, v_7^{-l_7}; J, -k\rangle \right\} , \end{aligned} \quad (4a)$$

$$|v_s, 0^0, 0^0, 0^0; J, 0\rangle_e = |v_s, 0^0, 0^0, 0^0; J, 0\rangle . \quad (4b)$$

161 The upper and lower signs (\pm) correspond to e and f wave-functions [36], respectively. For Σ states
 162 ($k = 0$), the first non-zero l_t is chosen positive.

163 4.1. Global fit

164 The analysis of the extended ro-vibrational data set has been performed following the same procedure
 165 described in details in Paper I. A total number of 533 rotational transitions and approximately 11 000 infrared
 166 lines have been added to the existing collection which now comprises a total number of 17 096 data. As
 167 usual, different weighting factors, $w = 1/\sigma^2$, have been used to take into account the unequal measurement
 168 precision (σ) of the various sources of data. The σ values for the new infrared data measured in this work
 169 are reported in the rightmost column of Table 1. For pure rotational lines, we retained the original weights
 170 of the literature data and used $\sigma = 15$ kHz for the newly measured transitions. The new data collected in
 171 the present work are summarised in Table 2.

172 The iterative fit procedure yields effective spectroscopic constants for each individual state, plus a set of
 173 interaction coefficients describing the accidental anharmonic resonances between nearly-degenerate vibra-
 174 tional states. Compared to our previous global fit, we determined the vibrational energy and the spectro-
 175 scopic parameters for 4 new vibrational states, namely $v_4 = v_7 = 1$, $(v_6 = 2, v_7 = 1)$, $(v_5 = 1, v_7 = 2)$,
 176 and v_5 , plus 10 more resonance coefficients. In addition, the states $v_1, v_2, v_3, v_1 = v_7 = 1, v_3 = v_7 = 1$,
 177 $v_3 = v_7 = 1$, already studied in Ref. [23] have been included in the present global analysis. For the constants
 178 which could not be directly determined from the fit procedure, we adopted suitable constraints. These
 179 have been derived from other states belonging to the same manifold assuming, whenever feasible, a linear
 180 v -dependence. This approach is implemented into the fitting code as described in Paper I and the whole
 181 procedure was repeated until the convergence of such derived values was achieved .

182 As briefly introduced in § 4, in HC_3N each level of the v_4 manifold is the pivot of the polyad of interacting
 183 states: $v_4 \sim (v_4 - 1, v_6 + 2) \sim (v_4 - 1, v_5 + 1, v_7 + 1) \sim (v_4 - 1, v_5 + 4)$. The fundamental polyad centered at
 184 $\sim 880 \text{ cm}^{-1}$ has been discussed in Paper I; in the following, we refer to it as the first resonance system (I RS).
 185 In this paper we investigated the polyad located at $\sim 1100 \text{ cm}^{-1}$ which includes the states $v_4 = v_7 = 1$,
 186 $(v_6 = 2, v_7 = 1)$, $(v_5 = 1, v_7 = 2)$, and $v_7 = 5$ (second resonance system, II RS, hereafter). In such a
 187 coupling scheme, a cubic interaction takes place between the $v_4 = v_7 = 1$ Π states and the Π sublevels of
 188 the $(v_6 = 2, v_7 = 1)$ and $(v_5 = 1, v_7 = 2)$ bend-bend combination; also a weak quintic **interaction** exists
 189 between $v_4 = v_7 = 1$ and $v_7 = 5$ states ($\Pi - \Pi$). In addition, the $(v_5 = 1, v_7 = 2)$ and $v_7 = 5$ states are
 190 coupled by a quartic resonance which produces effects on all their Π, Φ sublevels. The detailed scheme of
 191 the energy-level manifolds involved in this resonance system is depicted in Figure 4.

192 A remarkable feature of the II RS is the close vicinity of the $(v_5 = 1, v_7 = 2)$, and $v_7 = 5$ states which are
 193 coupled by the \tilde{H}_{40} Hamiltonian term. The resulting perturbations **affect** both Π and Φ sub-levels, and the

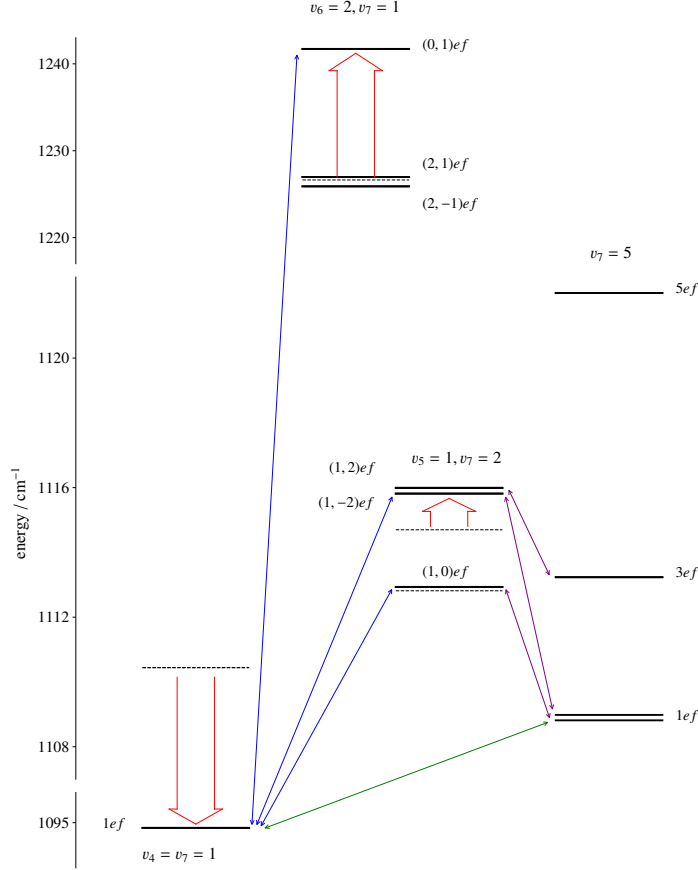


Figure 4: Vibrational energy diagram for the interacting states $v_4 = v_7 = 1$, $(v_6 = 2, v_7 = 1)$, $(v_5 = 1, v_7 = 2)$, and $v_7 = 5$ of HC_3N . Thin arrows indicate the main vibrational couplings relative to $\Delta k = 0$ taken into account: blue, green, and purple colors are associated to cubic (\tilde{H}_{30}), quartic (\tilde{H}_{40}), and quintic (\tilde{H}_{50}) interactions, respectively. Large arrows (red) illustrate the vibrational energy displacements produced by the anharmonic resonances; the unperturbed level positions are plotted with dashed lines. The weak $\Delta k = \pm 2$ interactions produced by the \tilde{H}_{32} and \tilde{H}_{42} Hamiltonian terms are not indicated.

194 corresponding lines show increasing differences from their unperturbed positions, as J approaches the value
 195 at which a given pair of interacting sublevels comes close to an exact degeneration. This is well illustrated in
 196 Figure 5 that plots the rotational energy trends for all the $(v_5 = 1, v_7 = 2)$ and $v_7 = 5$ level manifolds. The
 197 region around $J = 40$ has been extensively sampled in this work. Here the $(1, -2)^{ef}$ and $(1, 2)^{ef}$ levels of the
 198 $(v_5 = 1, v_7 = 2)$ state (here defined by the l_5 and l_7 quantum numbers only) become nearly-degenerate with
 199 the $l_7 = 3^{ef}$ levels of the $v_7 = 5$ manifold. Due to the avoided crossings, displacements up to ~ 4 GHz have
 200 been measured for some highly-perturbed lines and 10 transitions, formally labelled as “inter-state”, could
 201 also be observed. A very localised anomaly is also present at $J = 12$ in the manifold of the $(v_5 = 1, v_7 = 2)$
 202 combination. Here the $(1, 2)^e$ and the $(1, -2)^e$ sublevels, which are almost exactly degenerate, are heavily
 203 mixed because of the $\Delta k = \pm 2$ l -type resonance. As a result, two additional *intra-state* cross-over lines are
 204 generated, having half the relative intensity of the unperturbed ones. It should be underlined that, when

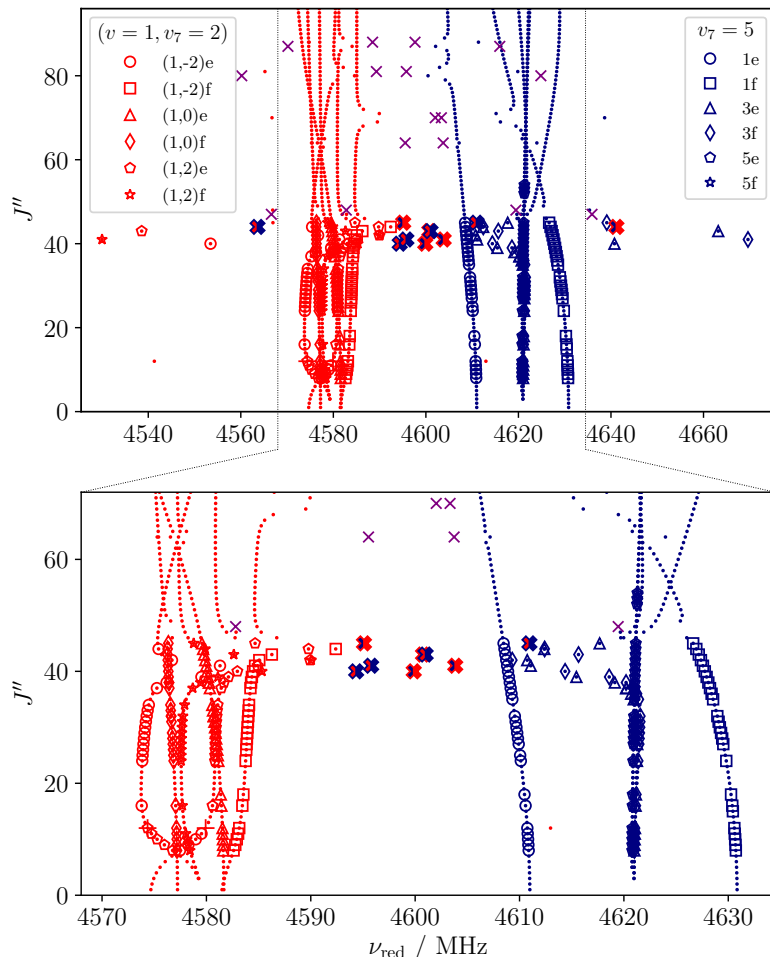


Figure 5: Reduced frequency diagram for the $(v_5 = 1, v_7 = 2)$, (red symbols) and $v_7 = 5$ (blue symbols) interacting states of HC_3N . The quantity plotted on the x -axis is $\nu_{\text{red}} = [\nu + 4D_0(J'' + 1)^3]/2(J'' + 1)$, where $D_0 = -0.5443$ kHz (ground-state value). Open symbols denote experimental values, whereas small dots indicate calculated values based on the parameters of Tables 3-8. Filled crosses label measured inter-state cross-over transitions, while the purple “times” symbols (\times) are used for those predicted by the actual model. The “plus” signs ($+$) are used for the $(v_5 = 1, v_7 = 2)$ intra-state $(1, 2)^e/(1, -2)^e$ cross-overs occurring at $J'' = 12$. The most perturbed transitions are labelled using the method implemented in the SPFIT code [37]. The bottom panel shows a detail of the upper plot in the ν_{red} range from 4568 to 4634 MHz.

205 a strong mixing between blocks of ro-vibrational wave-functions occurs, the labelling of the corresponding
 206 transitions become ambiguous. Our analysis tool, which uses SPFIT as the core computation routine, follows
 207 the method described by Pickett in Ref. [37].

208 As was the case for the I RS, we were able to completely analyse the II RS without any assumption on
 209 the energy position of the interacting levels. The network of resonances has been modelled with the same
 210 terms adopted for the I RS, the only addition being the C_{32} parameters which connects the $v_4 = v_7 = 1$
 211 and $(v_5 = 1, v_7 = 2)$ sublevels with $\Delta k = \pm 2$. The final fit returned a weighted root-mean-square (rms)

212 of $\sigma_w = 1.098$ thus indicating that, on average, the totality of the analysed data have been reproduced
 213 within the estimated experimental uncertainties. The complete list of the fitted transitions and their *obs-*
 214 *calc* residuals has been deposited as supplementary material. The optimised spectroscopic constants and
 215 resonance parameters are reported in Table 3–8.

Table 3: Spectroscopic constants derived for HC₃N in the ground and Σ^+ excited states.

Constant	Unit	Ground state	$v_4 = 1$	$v_3 = 1$	$v_2 = 1$	$v_1 = 1$
G_v	cm ⁻¹		878.315(21)	2079.306095(63)	2273.994846(61)	3327.371368(61)
B_v	MHz	4549.058599(35)	4538.0994(25)	4535.1154(16)	4527.4931(15)	4541.7750(14)
D_v	kHz	0.544252(11)	0.545441(97)	0.54115(24)	0.53795(20)	0.54017(19)
H_v	mHz	0.0501(14)	0.0373(23)	0.0501 ^a	0.0501 ^a	0.0501 ^a
L_v	nHz	-0.299(49)	-0.299 ^a	-0.299 ^a	-0.299 ^a	-0.299 ^a

Numbers in parentheses are one standard deviation in units of the last quoted digit.

^a Kept fixed to ground state value.

Table 4: Spectroscopic constants derived for HC₃N in Π singly-excited bending states.

Constant	Unit	$v_7 = 1$	$v_6 = 1$	$v_5 = 1$
G_v	cm ⁻¹	221.8376749(38)	498.7318990(52)	663.3685022(99)
$x_{L(tt)}$	GHz	21.823719768	6.64 ^a	...
$y_{L(tt)}$	MHz	-1.9539208
B_v	MHz	4563.525607(54)	4558.301833(61)	4550.62389(12)
D_v	kHz	0.568213(10)	0.554432(11)	0.545816(19)
H_v	mHz	0.10844(55)	0.06383(61)	0.04891(95)
L_v	nHz	-0.299 ^b	-0.299 ^b	-0.299 ^b
$d_{JL(tt)}$	kHz	-12.3148 ^a	12.3200 ^a	...
$h_{JL(tt)}$	Hz	0.03606 ^a
$l_{JL(tt)}$	μ Hz	-4.33 ^a
q_t	MHz	6.5386416(69)	3.5821933(50)	2.53861(11)
q_{tJ}	Hz	-16.2807(47)	-2.0650(21)	-1.3352(78)
q_{tJJ}	μ Hz	56.55(38)

Numbers in parentheses are one standard deviation in units of the last quoted digit.

^a Assumed value, see text.

^b Kept fixed to ground state value.

Table 5: Spectroscopic constants derived for HC₃N in Π stretching–bending combination states.

Constant	Unit	$v_4 = v_7 = 1$	$v_3 = v_7 = 1$	$v_2 = v_7 = 1$	$v_1 = v_7 = 1$
G_v	cm ⁻¹	1103.5031(41)	2298.776906(58)	2493.649777(52)	3548.408143(63)
$x_{L(tt)}$	GHz	21.8235 ^a	21.8235 ^a	21.8235 ^a	21.8235 ^a
$y_{L(tt)}$	MHz	-1.955 ^a	-1.955 ^a	-1.955 ^a	-1.955 ^a
B_v	MHz	4552.4024(81)	4549.7337(20)	4541.9904(12)	4556.2057(17)
D_v	kHz	0.57387(33)	0.56679(41)	0.56164(15)	0.55491(29)
H_v	mHz	0.287(15)	0.1092 ^a	0.1092 ^a	0.1092 ^a
L_v	nHz	-0.299 ^b	-0.299 ^b	-0.299 ^b	-0.299 ^b
$d_{JL(tt)}$	kHz	-12.3148 ^a	-12.3148 ^a	-12.3148 ^a	-12.3148 ^a
$h_{JL(tt)}$	Hz	0.03606 ^a	0.03606 ^a	0.03606 ^a	0.03606 ^a
$l_{JL(tt)}$	μ Hz	-4.33 ^a	-4.33 ^a	-4.33 ^a	-4.33 ^a
q_t	MHz	6.5551(18)	6.4572(24)	6.6500(15)	6.5426(21)
q_{tJ}	Hz	-17.293(60)	-14.95(61)	-18.27(24)	-17.33(46)
q_{tJJ}	μ Hz	56.55 ^a	56.55 ^a	56.55 ^a	56.55 ^a

Numbers in parentheses are one standard deviation in units of the last quoted digit.

^a Assumed value, see text.

^b Kept fixed to ground state value.

Table 6: Spectroscopic constants derived for HC₃N in bending overtone states.

Constant	Unit	$v_7 = 2$	$v_7 = 3$	$v_7 = 4$	$v_7 = 5$	$v_6 = 2$
G_v	cm ⁻¹	442.8985684(47)	663.2245907(88)	882.85094(25)	1101.828055(78)	997.905(20)
$x_{L(tt)}$	GHz	21.633441(35)	21.449844(33)	21.2833(19)	21.06947(24)	6.64(15)
$y_{L(tt)}$	MHz	-1.955 ^a	-1.955 ^a	-1.955(88)	-0.3497(62)	...
B_v	MHz	4577.967127(70)	4592.38377(12)	4606.77415(34)	4621.15002(20)	4567.4545(19)
D_v	kHz	0.5926296(98)	0.617401(24)	0.642542(19)	0.668160(46)	0.564555(16)
H_v	mHz	0.16383(50)	0.2168(13)	0.2678(10)	0.3217 ^a	0.07550(90)
L_v	nHz	-0.299 ^b	-0.299 ^b	-0.299 ^b	-0.299 ^b	-0.299 ^b
$d_{JL(tt)}$	kHz	-13.254(20)	-14.076(18)	-14.794(22)	-15.954(11)	12.32(48)
$h_{JL(tt)}$	Hz	0.0549(16)	0.0819(37)	0.1028(20)	0.1196(27)	...
$l_{JL(tt)}$	μHz	-3.96 ^a	-3.58(20)	-3.20(11)	-2.82 ^a	...
q_t	MHz	6.563420(91)	6.587570(26)	6.612141(46)	6.635470(84)	3.5821947 ^a
q_{tJ}	Hz	-16.623(17)	-16.9246(86)	-17.270(11)	-17.379(28)	-2.0650 ^a
q_{tJJ}	μHz	55.41(88)	54.92(57)	55.62(63)	54.81 ^a	...
w_{77}	Hz	-0.11185 ^a	-0.10874(37)	-0.10560(49)	-0.0720(33)	...

Numbers in parentheses are one standard deviation in units of the last quoted digit.

^a Assumed value, see text.

^b Kept fixed to ground state value.

Table 7: Spectroscopic constants derived for HC_3N in bending combination states.

Constant	Unit	$v_6 = v_7 = 1$	$v_6 = 1, v_7 = 2$	$v_6 = 2, v_7 = 1$	$v_5 = v_7 = 1$	$v_5 = 1, v_7 = 2$
G_v	cm^{-1}	720.2880301(52)	941.068193(20)	1219.179425(99)	885.37212(74)	1106.6535(14)
$x_L(\#\#)$	GHz	6.64 ^a	6.64 ^a	6.64 ^a
$x_L(\tau\tau)$	GHz	21.82354 ^a	21.66088(22)	21.82354 ^a	21.82354 ^a	21.7050(11)
$y_L(\tau\tau)$	MHz	-1.955 ^a	-1.955 ^a	-1.955 ^a	-1.955 ^a	-1.955 ^a
$x_L(\tau\tau)$	GHz	17.12559(10)	17.12588(13)	17.1062(13)	19.248(23)	18.322(20)
$r_{\tau\tau}$	GHz	-11.77215(14)	-11.49987(62)	-12.2727(42)	7.058(46)	8.999(40)
$r_{\tau J}$	kHz	-12.725(66)	-9.810(97)	-12.725 ^a	-0.0269(16)	-68.4(26)
$r_{\tau J J}$	Hz	1.829(80)	2.091(16)	1.829 ^a	1.02(10)	1.01 ^a
B_v	MHz	4572.864613(61)	4587.39084(16)	4582.11183(11)	4565.08437(95)	4579.4837(28)
D_v	kHz	0.578247(11)	0.602593(11)	0.587720(33)	0.569732(25)	0.592232(83)
H_v	mHz	0.13130(67)	0.19702(64)	0.04996 ^a	0.10621(76)	0.10628 ^a
L_v	nHz	-0.299 ^b	-0.299 ^b	-0.299 ^b	-0.299 ^b	-0.299 ^b
$d_{JL}(\#\#)$	kHz	12.3200 ^a	12.3200 ^a	12.3200 ^a
$d_{JL}(\tau\tau)$	kHz	-12.3148 ^a	-6.477(56)	-12.3148 ^a	-12.3148 ^a	-19.49(17)
$b_{JL}(\tau\tau)$	Hz	0.03606 ^a	0.03606 ^a	0.03606 ^a	0.03606 ^a	0.05760 ^a
$l_{JL}(\tau\tau)$	μHz	-4.3349 ^a	-4.3349 ^a	-4.3349 ^a	-4.3349 ^a	-3.9556 ^a
$d_{JL}(\tau\tau)$	kHz	55.652(83)	50.390(46)	55.186(68)	-20.22(72)	6.5(13)
$b_{JL}(\tau\tau)$	Hz	0.90(12)	0.90 ^a
$q_{\#}$	MHz	3.62252(40)	3.67226(27)	3.62253 ^a	2.56559(26)	2.5607(13)
$q_{\#J}$	Hz	-2.2691 ^a	-2.4735(94)	-2.0645 ^a	-1.439(11)	-1.439 ^a
q_{τ}	MHz	6.59296(19)	6.61721(12)	6.63503(41)	6.53864 ^b	6.5552(11)
$q_{\tau J}$	Hz	-16.359(11)	-16.6393(67)	-16.427(99)	-16.281 ^b	-16.840(71)
$q_{\tau J J}$	μHz	56.55 ^a	55.41 ^a	56.55 ^a	56.55 ^b	56.55 ^a
$u_{\tau\tau}$	Hz	...	-0.0909(28)
$u_{\tau J}$	Hz	-2.008(83)	-2.317(16)	-0.073(20)	-1.00(13)	-0.912(81)
$q_{\tau\tau\tau}$	kHz	...	-14.846(64)	-2.218(54)

Numbers in parentheses are one standard deviation in units of the last quoted digit.

^a Assumed value, see text.

^b Kept fixed to ground state value.

Table 8: Resonance parameters.

Interacting states	Parameter	Unit	Value
$(v_5 = 1) - (v_7 = 3)$	C_{40}	MHz	791.17(98)
$(v_5 = 1) - (v_7 = 3)$	C_{42}^J	MHz	-0.0253(30)
$(v_5 = v_7 = 1) - (v_7 = 4)$	C_{40}	MHz	742.2(51)
$(v_5 = v_7 = 1) - (v_7 = 4)$	C_{42}^J	MHz	0.1339(67)
$(v_4 = 1) - (v_6 = 2)$	C_{30}	cm^{-1}	16.0313(95)
$(v_4 = 1) - (v_6 = 2)$	C_{32}^J	MHz	-0.5164(23)
$(v_4 = 1) - (v_5 = v_7 = 1)$	C_{30}	cm^{-1}	-2.4109(40)
$(v_4 = 1) - (v_7 = 4)$	C_{50}	MHz	3498(29)
$(v_4 = 1) - (v_7 = 4)$	C_{52}^J	kHz	35.4(14)
$(v_5 = v_7 = 1) - (v_7 = 4)$	C_{42a}	kHz	21.08(84)
$(v_5 = v_7 = 1) - (v_7 = 4)$	C_{42b}	kHz	8.33(51)
$(v_5 = 1, v_7 = 2) - (v_7 = 5)$	C_{40}	MHz	938.0(32)
$(v_5 = 1, v_7 = 2) - (v_7 = 5)$	C_{42}^J	MHz	-0.0283(17)
$(v_4 = 1, v_7 = 1) - (v_6 = 2, v_7 = 1)$	C_{30}	cm^{-1}	15.94393(30)
$(v_4 = 1, v_7 = 1) - (v_6 = 2, v_7 = 1)$	C_{32}^J	MHz	-0.53450(52)
$(v_4 = 1, v_7 = 1) - (v_5 = 1, v_7 = 2)$	C_{30}	cm^{-1}	-2.2338(33)
$(v_4 = 1, v_7 = 1) - (v_5 = 1, v_7 = 2)$	C_{32}^J	MHz	-0.0626(65)
$(v_4 = 1, v_7 = 1) - (v_7 = 5)$	C_{50}	MHz	2825.8(30)
$(v_5 = 1, v_7 = 2) - (v_7 = 5)$	C_{42a}	kHz	1.11(18)
$(v_5 = 1, v_7 = 2) - (v_7 = 5)$	C_{42b}	kHz	-3.917(88)
$(v_4 = 1, v_7 = 1) - (v_5 = 1, v_7 = 2)$	C_{32}	kHz	-18.8(16)

Numbers in parentheses are one standard deviation in units of the last quoted digit.

216 *4.2. Ab initio calculations*

217 Very accurate predictions of molecular structures as well as of spectroscopic properties can be obtained
 218 by combining calculations at the coupled-cluster (CC) level of theory, with single and double excitations
 219 augmented by a perturbative treatment of triple excitations, i.e. CCSD(T) [38], within composite schemes for
 220 incorporating both the basis-set truncation and core-correlation effects. In the present work, the equilibrium
 221 structure of HC₃N has been obtained by applying the approach based on the additivity of the most relevant
 222 terms directly to the geometrical parameters (see, for example, [39, 40, 41]). Complete basis set (CBS)
 223 extrapolations were performed for both the Hartree-Fock self-consistent-field (HF-SCF) energy and the
 224 CCSD(T) correlation energy within the frozen-core (fc) approximation, employing the formulas of Halkier
 225 et al. [42] for the former, while the two-parameter correction of Helgaker et al. [43] was used for the latter.
 226 The correlation-consistent polarised basis sets cc-pVnZ ($n=Q,5,6$) by Dunning et al. [44, 45] were used,
 227 with $n=Q,5,6$ for HF-SCF and $N=Q,5$ for CCSD(T). The core-valence (CV) correlation term was computed
 228 (at the CCSD(T) level of theory) as the difference between the all-electron (ae) and frozen-core data using
 229 the cc-pCVQZ basis set [45]. By combining the CBS and CV terms, the best-estimate geometry, hereafter
 230 referred to as CCSD(T)/CBS+CV, was obtained. All the calculations were carried out using the CFOUR
 231 suite of programs [46] and its implementation of analytic second derivatives [47], while the anharmonic
 232 contributions to vibrational data and spectroscopic constants were calculated within the framework of 2nd-
 233 order vibrational perturbation theory (VPT2) and using an appropriate suite of programs [48] implementing
 234 the formulas reported in the literature (see Refs. [49, 50, 51]). The cubic and quartic semi-diagonal force
 235 constants needed to obtain these corrections were calculated at the fc-CCSD(T) level of theory and using
 236 the cc-pVQZ basis set.

237 The comparison between a selection of ab initio computed parameters and the corresponding experi-
 238 mental values are reported in Table 9. They include, vibration-rotation interaction constants (α_r), l -type
 239 doubling coefficients (q and q_J), anharmonicity constants ($x_{L(tt')}$), and vibrational l -type doubling param-
 240 eters ($r_{tt'}$). The agreement between experimentally derived and ab initio computed values is excellent for
 241 all the ro-vibrational parameters, except for α_4 , ($\sim 5\%$), α_5 , ($\sim 9\%$), q_5 , ($\sim 5\%$), and q_{5J} , ($\sim 30\%$).
 242 These constants are derived from vibrational fundamentals affected by anharmonic resonances ($v_4 = 1$ and
 243 $v_5 = 1$), thus their experimental values may include spurious contributions, not completely removed by the
 244 variational treatment.

245 It is worthwhile to note that our best-estimate geometry is in remarkable agreement with the semi-
 246 experimental equilibrium structure determined by Botschwina [22]. Actually, the comparison between our
 247 values ($r_{\text{HC}} = 1.0624 \text{ \AA}$, $r_{\text{CC}} = 1.2049 \text{ \AA}$, $r_{\text{CC}} = 1.13776 \text{ \AA}$ and $r_{\text{CN}} = 1.1606 \text{ \AA}$) and those of Ref. [22]
 248 ($r_{\text{HC}} = 1.0623 \text{ \AA}$, $r_{\text{CC}} = 1.2059 \text{ \AA}$, $r_{\text{CC}} = 1.3761 \text{ \AA}$ and $r_{\text{CN}} = 1.1606 \text{ \AA}$) points out an average error around
 249 0.7 m\AA with a maximum deviation of 1.5 m\AA .

250 Focusing on the vibrational anharmonicity constants, it should be noted that some of the $x_{L(tt')}$ and $r_{tt'}$
 251 coefficients contain near-singular denominators in their VPT2 formulation when $\omega_s \approx 2\omega_t$ or $\omega_s \approx \omega_t + \omega_{t'}$
 252 [49]. Such terms should be removed from the theoretically computed constants in order to allow for a
 253 meaningful comparison with the values derived from the spectral analysis, in which the resonances are
 254 explicitly treated, thus yielding “deperturbed” Hamiltonian coefficients. These corrected parameters have
 255 been marked with an asterisk in Table 9 and the problematic terms have been factored out as follows:

$$x_{L(tt)} = x_{L(tt)}^* - \frac{1}{32} \phi_{stt}^2 (2\omega_t - \omega_s)^{-1}, \quad (5a)$$

$$x_{L(tt')} = x_{L(tt')}^* - \frac{1}{16} \phi_{stt'}^2 (\omega_t + \omega_{t'} - \omega_s)^{-1}, \quad (5b)$$

$$r_{tt'} = r_{tt'}^* + \frac{1}{8} \phi_{stt'}^2 (\omega_t + \omega_{t'} - \omega_s)^{-1}. \quad (5c)$$

256 As it can be seen, the experimental values of these anharmonic quantities compare generally well with
 257 their ab initio counterparts, but two cases of strong disagreement are present: $x_{L(66)}$ and r_{57} . Both these
 258 parameters derive from the analysis of heavily perturbed energy level manifold, thus they retain certain
 259 degree of effectiveness. From the theoretical side, it should be noted that the magnitude of the singular

260 terms expressed by Eq. (5a) and (5c) is large: contributions of about 100 GHz and 21 GHz have been removed
 261 from the VPT2 computed $x_{L(66)}$ and r_{57} , respectively, to obtain the final (actually smaller) deperturbed
 262 values. As a result, the theoretical estimates of these quantities should be regarded with caution as they are
 263 very sensitive to any small numerical inaccuracy in the involved quadratic and cubic potential constants.

Table 9: Comparison between experimental and calculated *ab initio* spectroscopic constants of HC₃N.

Constant	Unit	Experimental ^a	ab initio ^b
α_1	MHz	7.2836	7.030
α_2	MHz	21.5655	21.585
α_3	MHz	13.9432	13.765
α_4	MHz	10.9592	10.445
α_5	MHz	-1.5653	-1.714
α_6	MHz	-9.2432	-9.234
α_7	MHz	-14.4670	-14.389
q_5	MHz	2.5386	2.4052
q_6	MHz	3.5822	3.508
q_7	MHz	6.5386	6.425
q_{5J}	Hz	-1.34	-0.896
q_{6J}	Hz	-2.07	-1.81
q_{7J}	Hz	-16.28	-15.04
$x_{L(55)}$	GHz	...	159.1
$x_{L(66)}^*$	GHz	6.64	-29.53
$x_{L(77)}$	GHz	21.823	21.52
$x_{L(56)}$	GHz	...	0.0
$x_{L(57)}^*$	GHz	19.248	16.24
$x_{L(67)}$	GHz	17.126	17.15
r_{56}	GHz	...	50.07
r_{57}^*	GHz	7.058	4.44
r_{67}	GHz	-11.772	-11.69

^a From constants of Tables 3–8.

^b Derived from VPT2 formulas using the force constants computed at the fc-CCSD(T) level in conjunction with cc-pV5Z (harmonic) and cc-pVQZ (cubic and quartic force field) basis set. Asterisks denote deperturbed values (see text).

264 5. Line list

265 Given the importance of HC₃N as astrochemical tracer, the set of spectroscopic constants obtained from
 266 the global fit has been used to predict an extended line list of rest frequencies which includes all observed
 267 lines, both rotational and ro-vibrational, and many other transitions of both types that could be predicted
 268 within their expected experimental uncertainty. The line list of about 90 000 transitions was calculated in
 269 the region 0–3600 cm⁻¹ with 68 927 transitions from this list adapted for the HITRAN2020 database [52].

270 A coherent computation of the line relative intensities for a comprehensive data set as such described
271 in this work requires some care. More specifically, when dealing with the various sub-bands of a transition
272 involving multiply-excited bending states, one should consider the various numerical factors arising from
273 the different v_t, l_t excitation and from the symmetrised form of the rovibrational basis. The issue has been
274 already recognised in Ref. [53] and beforehand treated in some details by Fayt et al. [54]. In this latter work,
275 however, the formulation is specifically tailored for the ν_9 band systems of NC_4N and cannot be applied
276 directly to our HC_3N data set. The procedure adopted in this work to carry out accurate and consistent
277 intensity calculations is reported in detail in Appendix A.

278 Briefly, we derived the transition moment of a single ro-vibrational line from the only experimental
279 data available in literature, namely the integrated band intensities of Ref. [53]. As far as the pure rotational
280 transitions are concerned, DeLeon et al. [55] reported the experimental determination of the dipole moments
281 in the ground, $v_7=1$ and $v_6=1$ states. All dipole moments relative to rotational transitions in other excited
282 vibrational states were either derived from the experimental ones, when feasible, or fixed to the ground state
283 value. Such transition and dipole moments were used as input information for the SPCAT routines [37]
284 in order to obtain a calculated value for the intensities of all the transitions included in the database we
285 produced. The comparison with the intensity values [53] reported in HITRAN2016 database [56] shows a
286 substantial agreement. On the contrary, there is a discrepancy with the intensity of the ν_1 fundamental band
287 at $\sim 3\mu\text{m}$ (which was not provided in HITRAN2016) calculated in Ref. [57] to model cometary atmospheres.
288 The values from Ref. [57] are approximately three times greater than those derived in this work. Since our
289 calculations reproduce accurately the relative intensity of the observed infrared bands over a wide range and
290 they match the values reported in HITRAN2016 for the FIR bands, we are confident about their reliability.

291 6. Conclusions

292 In this paper we present the most detailed and extended analysis of the rotational and high-resolution
293 ro-vibrational spectra of HC_3N to date. All fundamental bands and a considerable number of hot and
294 combination bands have been observed experimentally. A global fit including all transitions already published
295 and the new set of far infrared and rotational data has been performed and a very accurate set of rotational,
296 centrifugal distortion, vibrational, and l -doubling parameters has been obtained. Moreover, two networks of
297 anharmonic resonances have been observed and included in the total Hamiltonian. Their analysis has allowed
298 the determination of 21 resonance constants. A number of spectroscopic constants have been calculated from
299 an *ab initio* anharmonic force field. Their agreement with the corresponding experimental parameters is
300 very good.

301 About 90 000 rotational and ro-vibrational transition energies have been predicted on the basis of the
302 molecular constants obtained from the global fit. This calculated database includes a large number of
303 unobserved transitions, which however were confidently predicted within their expected average experimental
304 uncertainty. Intensity calculations have been performed for all the lines of the database. If compared to the
305 HITRAN2016 database, the ro-vibrational intensities show a general agreement. As far as the rotational
306 lines are concerned, the new database HITRAN2020, which includes our line list, contains a much larger
307 number of transitions. Also, some sets of transitions mislabelled or with a wrong intensity value have been
308 corrected.

309 Although the line list in HITRAN2016 [56] includes almost 180 000 transitions, no ro-vibrational data
310 are present below 463.6 cm^{-1} or above 759.0 cm^{-1} . Therefore, our list is more complete in terms of total
311 spectral window, since it covers all vibrational modes. It is less complete in terms of vibrational transitions,
312 as hot and combination bands involving highly excited vibrational states were not considered because of
313 their negligible intensity. The HITRAN2020 edition of the database [52] now employs our line list below
314 463.6 cm^{-1} and above 759.0 cm^{-1} .

315 In conclusion, this paper provides an accurate and precise set of spectroscopic constants for HC_3N , which
316 can be used to test high level *ab initio* calculations. Moreover, a reliable list of rest frequencies and intensities
317 is presented. This database is of considerable importance when the detailed and quantitative interpretation
318 of spectra of remote environments, such as planetary atmospheres or any other space environment is required.

319 7. Acknowledgement

320 This study was supported by Bologna University (RFO funds). This work has been performed under the
 321 SOLEIL proposal #20190128; we acknowledge the SOLEIL facility for provision of synchrotron radiation
 322 and would like to thank the AILES beamline staff for their assistance. Support by the Italian Space Agency
 323 (ASI; ‘Life in Space’ project, N. 2019-3-U.0) is also acknowledged. J.-C.G. thanks the Centre National
 324 d’Etudes Spatiales (CNES) for a grant. A.P.C. gratefully acknowledges financial support by University
 325 Ca’ Foscari Venezia (ADiR funds) and the computational facilities of the SCSCF (“Sistema per il Calcolo
 326 Scientifico di Ca’ Foscari”). B.M.G. and P.C. acknowledge the support of the Max-Planck-Society. IEG
 327 contribution was supported through NASA grant 80NSSC20K1059. We thank Ekaterina Karlovets for her
 328 help with validating early versions of the line list.

329 Appendix A. Intensity calculation

330 The experimental integrated band intensities are reported in Tables 1 and 2 of Ref. [53]. A theoretical
 331 description for such quantity can be derived from the expression of an individual ro-vibrational transition
 332 $a, J' \leftarrow b, J''$ (J is the rotational quantum number and a and b summarize all other quantum numbers) of
 333 a bulk system of N molecules at temperature T .

$$I_{\text{rv}}^N(T) = \frac{\gamma_i \pi \nu_{\text{rv}} n_{\text{L}} T_0}{p_0 T} \frac{S_{aJ', bJ''}}{3\epsilon_0 \hbar c} \frac{e^{-E''_{\text{rv}}/kT} (1 - e^{-h\nu_{\text{rv}}/kT})}{Q_{\text{rv}}(T)}, \quad (\text{A.1})$$

334 where ν_{rv} is the transition frequency, γ_i the isotopic fractional abundance, $Q_{\text{rv}}(T)$ the total rovibrational
 335 partition function at T , n_{L} the Loschmidt number at $p_0 = 1$ atm and $T_0 = 273.15$ K, E''_{rv} is the energy of
 336 the lower state and $S_{aJ', bJ''}$ the line strength. $S_{aJ', bJ''}$ can be factored as follows:

$$S_{aJ', bJ''} = \Theta_{ab}^2 L(J', J'', k', k'') W_{ab}, \quad (\text{A.2})$$

337 in which Θ_{ab} is the dipole moment derivative for the $a \leftarrow b$ vibrational transition, $L(J', J'', k', k'')$ the
 338 Hönl-London factor and W_{ab} is a numerical factor. $S_{aJ', bJ''}$ will be discussed in more detail later. By
 339 re-elaborating Eq. (A.1) we obtain

$$I_{\text{rv}}^N(T) = \frac{8\pi^3 n_{\text{L}} T_0}{3p_0 \hbar c} \frac{1}{4\pi\epsilon_0} \gamma_i \nu_{\text{rv}} \Theta_{ab}^2 W_{ab} \frac{L(J', J'', k', k'') e^{-E''_{\text{rv}}/kT} (1 - e^{-h\nu_{\text{rv}}/kT})}{Q_{\text{r}}(T)} \frac{e^{-E''_{\text{v}}/kT}}{T Q_{\text{v}}(T)}. \quad (\text{A.3})$$

340 In the expression above we assumed $E_{\text{rv}} = E_{\text{v}} + E_{\text{r}}$, and $Q_{\text{rv}}(T) = Q_{\text{v}}(T) Q_{\text{r}}(T)$. In order to obtain the
 341 integrated band intensity we need to sum over all possible transitions (P , Q and R) of a given band starting
 342 from any initial level defined by J'' . Namely

$$I_{\text{rv}}(T) = \sum_{J''} \sum_{P, Q, R} I_{\text{rv}}^N(T). \quad (\text{A.4})$$

343 Considering that

$$\sum_{P, Q, R} L(J', J'', k', k'') = 2J'' + 1, \quad (\text{A.5a})$$

$$\sum_{J''} \frac{2J'' + 1}{Q_{\text{r}}(T)} e^{-E''_{\text{r}}/kT} = 1, \quad (\text{A.5b})$$

344 equation (A.4) can be written as

$$I_{\text{rv}}(T) = \frac{8\pi^3 n_{\text{L}} T_0}{3p_0 \hbar c} \frac{1}{4\pi\epsilon_0} \gamma_i \nu_0 \Theta_{ab}^2 W_{ab} \frac{(1 - e^{-h\nu_0/kT})}{T Q_{\text{v}}(T)}, \quad (\text{A.6})$$

345 where all rotational terms have been removed. The constants in equation (A.6) are taken from CODATA 2018
 346 [58] and are: $n_L = 2.686780111 \times 10^{19} \text{ mol cm}^{-3}$, $T_0 = 273.15 \text{ K}$, $p_0 = 1 \text{ atm}$, $h = 6.62607015 \times 10^{-27} \text{ erg s}$,
 347 $c = 2.99792458 \times 10^{10} \text{ cm s}^{-1}$, $1/4\pi\epsilon_0 = 10^{-36} \text{ erg cm}^3 \text{ D}^{-2}$. Since Θ_{ab}^2 is measured in D^2 and ν_0 in cm^{-1} ,
 348 the intensity is expressed in units of $\text{cm}^{-2} \text{ atm}^{-1}$. Moreover, we can safely assume that ν_{rv} is equal to the
 349 band origin ν_0 . The purely vibrational exponential is equal to 1, as the ground state vibrational energy is
 350 set to zero. By substitution of the above constants we eventually have:

$$I_{rv}(T) = 3054.74207 \gamma_i \nu_0 \Theta_{ab}^2 W_{ab} \frac{(1 - e^{-h\nu_0/kT})}{T Q_v(T)}. \quad (\text{A.7})$$

351 The factor 3054.74207 is the same reported in Ref. [59]. If a band system is considered, the total intensity
 352 is given by a sum over all populated vibrational states obtained by multiplying $I_{rv}(T)$ by the vibrational
 353 partition function. We therefore obtain:

$$I_{rv}^{BS}(T) = 3054.74207 \gamma_i \nu_0 \Theta_{ab}^2 W_{ab} \frac{(1 - e^{-h\nu_0/kT})}{T}. \quad (\text{A.8})$$

354 $I_{rv}^{BS}(T)$ is directly comparable with the integrated band intensities given in Ref. [53].

355 The line strength of Eq. (A.2) gives rise to rotational and vibrational factors symbolically defined as L
 356 and W_{ab} . Following the procedure of Refs. [50, 60], the line strength of an allowed rovibrational transition
 357 ($a, J' \leftarrow b, J''$) can be expressed as

$$S_{aJ',bJ''} = \sum_{f,M',M''} |\langle aJ'M' | M_f | bJ''M'' \rangle|^2, \quad (\text{A.9})$$

358 where a and b collect all the quantum numbers not indicated explicitly (see later), and M_f are the space-fixed
 359 components of the electric dipole moment.

360 The following steps are then taken:

- 361 i. the dipole moment operator is expressed in terms of the molecule-fixed components μ_γ and the rotation
 362 matrices $\mathcal{D}_{f\gamma}^{(1)}(\omega)^*$ through $M_f = \sum_\gamma \mathcal{D}_{f\gamma}^{(1)}(\omega)^* \mu_\gamma$ [61];
- 363 ii. the dipole moment components μ_γ are expanded as a function of the normal coordinates q_r :
 364 $\mu_\gamma = \mu_e^\gamma + \sum_r \mu_r^\gamma q_r + \sum_{r,s} \mu_{rs}^\gamma q_r q_s + \dots = \mu_{00}^\gamma + \mu_{10}^\gamma + \mu_{20}^\gamma + \dots$; μ_r^γ and μ_{rs}^γ are the first and second
 365 derivatives of the dipole moment with respect to the normal coordinates;
- 366 iii. if only the μ_{10}^γ and μ_{20}^γ terms are maintained, the fundamental, overtone, combination, and difference
 367 bands with $\sum_r |\Delta v_r| = 2$ are accounted for, and the M_f components become $M_f = \mathcal{D}_{f\gamma}^{(1)}(\omega)^* \mu_{10}^\gamma +$
 368 $\mathcal{D}_{f\gamma}^{(1)}(\omega)^* \mu_{20}^\gamma = M_{11}^f + M_{21}^f$;
- 369 iv. the ro-vibrational wave-functions are factorised as $|aJM\rangle = \sum_{l,k} a_{vlk} |v,l\rangle |J,k,M\rangle$, where v and l
 370 represent all vibrational quantum numbers and $k = \sum_t l_t$.

371 The line strength expression thus becomes:

$$S_{aJ',bJ''} = \sum_{f,M',M''} \left| \langle aJ'M' | M_{11}^f + M_{21}^f | bJ''M'' \rangle \right|^2, \quad (\text{A.10a})$$

$$S_{aJ',bJ''} = \sum_{f,M',M''} \left| \sum_{l',l'',k',k''} a_{v'l'k'}^* b_{v''l''k''} \langle v',l' | \mu_{10}^\gamma + \mu_{20}^\gamma | v'',l'' \rangle \langle J',k',M' | \mathcal{D}_{f\gamma}^{(1)}(\omega)^* | J'',k'',M'' \rangle \right|^2. \quad (\text{A.10b})$$

372 By evaluating the integral over the rotation matrices, the sum over the space-fixed variables f, M', M'' , and
 373 applying the sum rules for the $3j$ -symbols, the intensity integral becomes [60]:

$$S_{aJ',bJ''} = \left| \sum_{k',k''} a_{v'l'k'}^* b_{v''l''k''} \langle v',l' | \mu_{10}^{k'-k''} + \mu_{20}^{k'-k''} | v'',l'' \rangle \right. \\ \left. \times [(2J'+1)(2J''+1)]^{1/2} \begin{pmatrix} J' & 1 & J'' \\ -k' & k'-k'' & k'' \end{pmatrix} \right|^2. \quad (\text{A.11})$$

374 The sum in Eq. (A.11) can include one, two, or four terms, because it runs over degenerate states described
375 by the symmetry-adapted basis functions defined in Eqs. (4). In this work, Eq. (A.11) has been implemented
376 in a automatic routine that computes the vibrational intensity factors using the appropriate symmetrised
377 basis functions.

378 As already mentioned, the dipole moment operators in Eq. (A.11) will apply to different vibrational
379 transitions: M_{11}^f to the fundamental bands and M_{21}^f , to the first overtones, combinations, and difference
380 bands. Their dependence from the vibrational coordinates can be conveniently expressed in terms of products
381 of the ladder operators [62]. For instance, the dipole moment for fundamental vibrational transitions is:

$$\mu_{10}^\gamma = \frac{1}{2} \sum_s \Theta_s \left(\hat{\mathcal{L}}_s^+ + \hat{\mathcal{L}}_s^- \right) + \sum_t \Theta_t \left[\left(\hat{\mathcal{L}}_{t,+}^+ - \hat{\mathcal{L}}_{t,-}^+ \right) + \left(\hat{\mathcal{L}}_{t,-}^- - \hat{\mathcal{L}}_{t,+}^- \right) \right], \quad (\text{A.12})$$

382 where Θ_r ($r = s, t$) is a coefficient proportional to the dipole moment derivatives and s and t denotes
383 non-degenerate (stretching) and doubly-degenerate (bending) normal modes, respectively. The sums of
384 operators above are needed to ensure that the operator is Hermitian. To give an example, the line strength
385 of a $J' \leftarrow J''$ P or R transition of the ν_7 fundamental perpendicular band can be derived from Eq. (A.12),
386 if we consider only the terms for $t = 7$, as

$$\mu_{10,7}^{(1)} = \Theta_7 \left(\hat{\mathcal{L}}_{7,+}^+ - \hat{\mathcal{L}}_{7,-}^+ + \hat{\mathcal{L}}_{7,-}^- - \hat{\mathcal{L}}_{7,+}^- \right), \quad (\text{A.13})$$

387 where $\mu^{(\pm 1)} = \mu_x \pm i\mu_y$ for the spherical components of the dipole moment operator. The wavefunctions of
388 the ro-vibrational states involved in the transition, described with a simplified notation of Eqs. (4) $|v_7, l_7\rangle$,
389 are $|0, 0\rangle$ for the ground state and $\frac{1}{\sqrt{2}} \{|1, 1\rangle - |1, -1\rangle\}$ for the upper state of e parity.

390 By substituting Eq. (A.13) in Eq. (A.11), the non-vanishing terms give rise to the following line strength
391 expression:

$$S_{\nu_7, J' \leftarrow J''} = \frac{(\Theta_7)^2}{2} \left| \left\{ \langle 1, 1 | \hat{\mathcal{L}}_{7,+}^+ | 0, 0 \rangle \begin{pmatrix} J' & 1 & J'' \\ -1 & 1 & 0 \end{pmatrix} + \langle 1, -1 | \hat{\mathcal{L}}_{7,-}^+ | 0, 0 \rangle \begin{pmatrix} J' & 1 & J'' \\ 1 & -1 & 0 \end{pmatrix} \right\} \right|^2 \\ \times (2J'+1)(2J''+1) = 2(\Theta_7)^2 (2J'+1)(2J''+1) \begin{pmatrix} J' & 1 & J'' \\ 1 & -1 & 0 \end{pmatrix}^2. \quad (\text{A.14})$$

392 The term involving only rotational quantum numbers is the Hönl-London factor. It can be shown, by
393 applying the algebraic expression of the $3j$ -symbols, that Eq. (A.14) is equivalent to Eqs. (24)–(26) of
394 Ref. [54] for the P, R branches¹.

395 The Θ_r, Θ_{rs} coefficients, used as input for the SPCAT routines [37], have been derived from the absolute
396 band intensities reported in Tables 1 and 2 of Ref. [53] by applying Eq. (A.8) and calculating the vibrational
397 factors W_{ab} for all the fundamentals and for some overtone and combination bands. The results of such
398 derivation are reported in Table A.10. The intensity perturbations produced by the various resonances have
399 been taken automatically into account by the SPCAT program.

400 Note that the following points should be taken into account in doing this calculation:

¹Note that a typo is present in Eq. (25) Ref. [54]. The correct formula for the $P(J)$ Hönl-London factors is reported in Eq. (13) of the same paper.

- 401 i. In Ref. [53] it is assumed that $\gamma_i = 1$ for all vibrational bands belonging to the same band system.
402 ii. The S_V^{BS} value reported for the ν_4 band is most likely to be the sum of ν_4 and $\nu_5 + \nu_7$ bands (in fact, the
403 same feature was assigned as $\nu_5 + \nu_7$ by Khlifi et al. [63]). These two bands are very weak and separated
404 by only $\sim 24 \text{ cm}^{-1}$, so that the R branch of ν_4 completely overlaps with the P branch of $\nu_5 + \nu_7$. Based
405 on our high-resolution measurements, we have estimated a relative intensity ratio $\nu_4:(\nu_5 + \nu_7)$ of 1:1.4
406 The reported value of $0.68 \text{ cm}^{-2} \text{ atm}^{-1}$ [53] has been then split between these two bands, accordingly.
407 iii. The $v_4 = 1$, $v_5 = v_7 = 1$, and $v_6 = 2$ states are involved in the I RS (see § 4.1) and the intensity of the
408 corresponding ν_4 , $\nu_5 + \nu_7$, and $2\nu_6$ band are altered by the wave-function mixing. Hence, the direct use
409 of the Θ_4 , Θ_{57} , and Θ_{66} derived via Eq. (A.8) and experimental intensity data would lead to incorrect
410 line intensity calculations. Deperturbed values (Θ_4^* , Θ_{57}^* , Θ_{66}^*) of these dipole moment derivatives have
411 been obtained via

$$\Theta^* = \Theta \tilde{\mathbf{V}} \quad (\text{A.15})$$

412 where $\Theta = (\Theta_4, \Theta_{57}, \Theta_{66})$ and $\tilde{\mathbf{V}}$ is the transpose eigenvector matrix of the vibrational Hamiltonian
413 which includes the $v_4 = 1$, $v_5 = v_7 = 1$, and $v_6 = 2$ states. The values of Θ_4^* , Θ_{57}^* , Θ_{66}^* are also reported
414 in Table A.10.

Table A.10: Transition moments of HC_3N .

band	Intensity ^a / $\text{cm}^{-2} \text{ atm}^{-1}$	W_{ab}	Θ_v ^b / 10^{-2} D
ν_1	249.4	1/2	12.05
ν_2	40.7	1/2	5.890
ν_3	8.0	1/2	2.73
ν_4	0.28 ^c	1/2	0.80 (1.16)
ν_5	268.6	2	14.30
ν_6	39.0	2	6.447
ν_7	0.73 ^d	2	1.55
$\nu_6 + \nu_7$	12.1	2	2.897
$\nu_5 + \nu_7$	0.40 ^c	2	0.75 (0.527)
$2\nu_6$	1.72	4	0.643 (0.546)

Notes:

- (a) From Ref. [53] except indicated otherwise.
(b) values in parentheses denote deperturbed values.
(c) Estimated from our experimental measurements (see text).
(d) From Ref. [64].

415 As far as the pure rotational transition intensities are concerned, DeLeon et al. [55] reported the ex-
416 perimental determination of the dipole moment in the ground ($\mu_0=3.73172(1) \text{ D}$), $v_7=1$ ($\mu_7=3.7225(2) \text{ D}$),
417 and $v_6=1$ ($\mu_6=3.7263(1) \text{ D}$) states. In order to derive a value of the dipole moment also for other excited
418 vibrational states observed in our rotational spectra, we expressed the dipole moment as a function of the
419 vibrational quantum numbers, $\mu_v = \mu_e - \sum_i \delta_i (v_i + \frac{d_i}{2})$. By analogy with the usual expansion in the vibra-
420 tional quantum numbers, μ_e is the equilibrium value of the dipole moment, δ_i are the expansion coefficients
421 and d_i the degeneracy of the i -th vibrational mode. In this fashion, a prediction of the dipole moment could
422 be calculated from the experimental values available for all vibrational states which involve excitation of
423 ν_6 and/or ν_7 . For example, $\mu_{67} = \mu_6 + \mu_7 - \mu_0 = 3.71708 \text{ D}$ and $\mu_{777} = 4\mu_7 - 3\mu_0 = 3.69484 \text{ D}$. Other
424 dipole moments that could not be derived from the experimental information were fixed to the ground state

425 value. This is clearly not correct but we estimated that the error introduced is in general well below 1% of
426 the value of the dipole moment. Ultimately, the final test of the goodness of the intensity predictions was
427 achieved by plotting the calculated spectrum against the experimental one. The consistency of the relative
428 intensity of the infrared bands and rotational transitions confirmed the accuracy of our derivations.

429 References

- 430 [1] B. Turner, Detection of interstellar cyanoacetylene, *Astrophys. J.* 163 (1971) L35.
431 [2] M. J. Mumma, S. B. Charnley, The chemical composition of comets—emerging taxonomies and natal heritage, *Ann. Rev.*
432 *Astron. Astrophys.* 49 (2011) 471–524.
433 [3] R. Mauersberger, C. Henkel, L. Sage, Dense gas in nearby galaxies. III- HC₃N as an extragalactic density probe, *Astron.*
434 *Astrophys.* 236 (1990) 63–68.
435 [4] V. Kunde, A. Aikin, R. Hanel, D. Jennings, W. Maguire, R. Samuelson, C₄H₂, HC₃N and C₂N₂ in Titan’s atmosphere,
436 *Nature* 292 (5825) (1981) 686–688.
437 [5] N. Yu, J.-J. Wang, J.-L. Xu, Chemical evolution of HC₃N in dense molecular clouds, *Mon. Not. R. Astron. Soc.* 489 (2019)
438 4497–4512. doi:10.1093/mnras/stz2431.
439 [6] V. Rivilla, L. Colzi, F. Fontani, M. Melosso, P. Caselli, L. Bizzocchi, F. Tamassia, L. Dore, DC₃N observations towards
440 high-mass star-forming regions, *Mon. Not. R. Astron. Soc.* 496 (2) (2020) 1990–1999.
441 [7] A. E. Thelen, C. A. Nixon, N. J. Chanover, M. A. Cordiner, E. M. Molter, N. A. Teanby, P. G. J. Irwin, J. Serigano, S. B.
442 Charnley, Abundance measurements of titan’s stratospheric HCN, HC₃N, C₃H₄, and CH₃CN from ALMA observations,
443 *Icarus* 319 (2019) 417–432. doi:10.1016/j.icarus.2018.09.023.
444 [8] P. B. Rimmer, L. Majumdar, A. Priyadarshi, S. Wright, S. Yurchenko, Detectable abundance of cyanoacetylene (HC₃N)
445 predicted on reduced nitrogen-rich super-earth atmospheres, arXiv preprint arXiv:2107.13097 (2021).
446 [9] J. R. Pardo, J. Cernicharo, J. R. Goicoechea, T. G. Phillips, The Slowly Expanding Envelope of CRL 618 Probed with
447 HC₃N Rotational Ladders, *Astroph. J.* 615 (1) (2004) 495–505. doi:10.1086/424379.
448 [10] F. Rico-Villas, J. Martín-Pintado, E. González-Alfonso, V. M. Rivilla, S. Martín, S. García-Burillo, I. Jiménez-Serra,
449 M. Sánchez-García, Vibrationally excited HC₃N emission in NGC 1068: tracing the recent star formation in the starburst
450 ring, *Mon. Not. R. Astron. Soc.* 502 (2) (2021) 3021–3034. doi:10.1093/mnras/stab197.
451 [11] L. Bizzocchi, F. Tamassia, J. Laas, B. M. Giuliano, C. Degli Esposti, L. Dore, M. Melosso, E. Canè, A. Pietropolli-Charmet,
452 H. S. P. Müller, H. Spahn, A. Belloche, P. Caselli, K. M. Menten, R. T. Garrod, Rotational and high-resolution infrared
453 spectrum of HC₃N: global ro-vibrational analysis and improved line catalog for astrophysical observations, *Astrophys. J.*
454 *Suppl. S.* 233 (2017) 11(20pp). doi:10.3847/1538-4365/aa9571.
455 [12] P. D. Mallinson, J. Fayt, High resolution infra-red studies of HCCCN and DCCCN, *Mol. Phys.* 32 (1976) 473–485.
456 doi:10.1080/00268977600103231.
457 [13] F. Winther, S. Klee, G. Mellau, S. Naïm, L. Mbosey, A. Fayt, The ν_1 band system of H–CC–CN (Cyanoacetylene), *J.*
458 *Mol. Spectrosc.* 175 (1996) 354–362. doi:10.1006/jmsp.1996.0040.
459 [14] K. Yamada, R. Best, G. Winnewisser, A. W. Mantz, Diode laser spectrum of HCCCN: CN stretching band, *Z. Naturforsch.*
460 *38a* (1983) 1296–1308. doi:10.1515/zna-1983-1205.
461 [15] K. Yamada, R. Schieder, G. Winnewisser, A. W. Mantz, Diode laser spectrum of HCCCN near 5 μm , *Z. Naturforsch.* 35a
462 (1980) 690–693. doi:10.1515/zna-1980-0705.
463 [16] K. Yamada, G. Winnewisser, Diode laser spectrum of HCCCN near 5 μm . The hot band, *Z. Naturforsch.* 36a (1981)
464 23–29. doi:10.1515/zna-1981-0105.
465 [17] A. Dargelos, C. Pouchan, CCSD(T)-F12 calculations of the IR spectrum of cyanoacetylene HC₃N beyond the harmonic
466 approximation, *Chem. Phys. Lett.* 754 (2020) 137746. doi:10.1016/j.cpllett.2020.137746.
467 [18] R. M. Vichiatti, R. L. A. Haiduke, The infrared fundamental intensities of some cyanopolynes, *Spectrochim. Acta A* 90
468 (2012) 1–11. doi:10.1016/j.saa.2012.01.005.
469 [19] T. A. Holme, J. S. Hutchinson, SCF calculation of the structure, force field, and dipole function of cyanoacetylene, *Chem.*
470 *Phys.* 93 (1985) 419–423. doi:10.1016/0301-0104(85)87006-3.
471 [20] J. S. Hutchinson, High-energy vibrational state of cyanoacetylene - variational and perturbative analysis of an anharmonic
472 normal mode, *J. Chem. Phys.* 82 (1985) 22–30. doi:10.1063/1.448795.
473 [21] P. Botschwina, B. Schulz, M. Horn, M. Matuschewski, Ab initio calculations of stretching vibrational transitions for the
474 linear molecules HCN, HNC, HCCF and HC₃N up to high overtones, *Chem. Phys.* 190 (1995) 345–362. doi:10.1016/
475 0301-0104(94)00350-J.
476 [22] P. Botschwina, Accurate equilibrium structures for small polyatomic molecules, radicals and carbenes, *Molecular Physics*
477 *103* (10) (2005) 1441–1460. doi:10.1080/00268970500070116.
478 [23] N. Jiang, M. Melosso, F. Tamassia, L. Bizzocchi, L. Dore, E. Canè, D. Fedele, J.-C. Guillemin, C. Pizzarini, High-resolution
479 infrared spectroscopy of DC₃N in the stretching region, *Front. Astron. Space Sci.* 8 (2021) 29.
480 [24] M. Melosso, L. Bizzocchi, A. Adamczyk, E. Cané, P. Caselli, L. Colzi, et al., Extensive ro-vibrational analysis of deuterated-
481 cyanoacetylene (DC₃N) from millimeter-wavelengths to the infrared domain, *J. Quant. Spectrosc. Ra.* 254 (2020) 107221.
482 [25] J.-B. Brubach, L. Manceron, M. Rouzières, O. Pirali, D. Balcon, F. Kwabia-Tchana, V. Boudon, M. Tudorie, T. Huet,
483 A. Cuisset, P. Roy, Performance of the AILES THz-Infrared beamline at SOLEIL for high resolution spectroscopy, WIRMS
484 2009 AIP Conf. Proc. 1214 (2009) 81–84. doi:10.1063/1.3326359.
485 [26] O. Pirali, V. Boudon, J. Oomens, M. Vervloet, Rotationally resolved infrared spectroscopy of adamantane, *J. Chem. Phys.*
486 *136* (2012) 024310. doi:10.1063/1.3666853.

- [27] O. Pirali, M. Goubet, T. R. Huet, R. Georges, P. Soulard, P. Asselin, J. Courbe, P. Roy, M. Vervloet, The far infrared spectrum of naphthalene characterized by high resolution synchrotron FTIR spectroscopy and anharmonic DFT calculations, *Phys. Chem. Chem. Phys.* 15 (2013) 10151–10150. doi:10.1039/c3cp44305a.
- [28] F. Matsushima, H. Odashima, T. Iwasaki, S. Tsunekawa, K. Takagi, Frequency-measurement of pure rotational transitions of H₂O from 0.5 to 5 THz, *J. Mol. Struct.* 352 (1995) 371–378. doi:10.1016/0022-2860(94)08531-L.
- [29] V. M. Horneman, R. Anttila, S. Alanko, J. Pietila, Transferring calibration from CO₂ laser lines to far infrared water lines with the aid of the ν_2 band of OCS and the ν_2 , $\nu_1 - \nu_2$, and $\nu_1 + \nu_2$ bands of ¹³CS₂: Molecular constants of ¹³CS₂, *J. Mol. Spectrosc.* 234 (2005) 238–254. doi:10.1016/j.jms.2005.09.011.
- [30] L. Bizzocchi, M. Melosso, L. Dore, C. Degli Esposti, F. Tamassia, D. Prudenzeno, V. Lattanzi, J. Laas, S. Spezzano, B. M. Giuliano, C. P. Endres, P. Caselli, Accurate Laboratory Measurement of the Complete Fine Structure of the N = 1 - 0 Transition of ¹⁵NH, *Astrophys. J.* 863 (1) (2018) 3. doi:10.3847/1538-4357/aacffc.
- [31] M. Melosso, B. Conversazioni, C. Degli Esposti, L. Dore, E. Cané, F. Tamassia, L. Bizzocchi, The pure rotational spectrum of ¹⁵ND₂ observed by millimetre and submillimetre-wave spectroscopy, *J. Quant. Spectrosc. Ra.* 222 (2019) 186–189.
- [32] M. Melosso, L. Bizzocchi, F. Tamassia, C. Degli Esposti, E. Cané, L. Dore, The rotational spectrum of ¹⁵ND. isotopic-independent Dunham-type analysis of the imidogen radical, *Phys. Chem. Chem. Phys.* 21 (2019) 3564–3573.
- [33] L. Dore, Using fast fourier transform to compute the line shape of frequency-modulated spectral profiles, *J. Mol. Spectrosc.* 221 (2003) 93–98. doi:10.1016/S0022-2852(03)00203-0.
- [34] R. V. Kochanov, I. Gordon, L. Rothman, P. Wcisło, C. Hill, J. Wilzewski, Hitran application programming interface (hapi): A comprehensive approach to working with spectroscopic data, *J. Quant. Spectrosc. Ra.* 177 (2016) 15–30.
- [35] K. M. T. Yamada, F. W. Birss, M. R. Aliev, Effective Hamiltonian for polyatomic linear molecules, *J. Mol. Spectrosc.* 112 (1985) 347.
- [36] J. M. Brown, J. T. Hougen, K.-P. Huber, J. W. C. Johns, I. Kopp, H. Lefebvre-Brion, A. J. Merer, D. A. Ramsay, J. Rostas, R. N. Zare, The labeling of parity doublet levels in linear molecules, *J. Mol. Spectrosc.* 55 (1975) 500.
- [37] H. M. Pickett, The fitting and prediction of vibration-rotation spectra with spin interactions, *J. Mol. Spectrosc.* 148 (2) (1991) 371–377.
- [38] K. Raghavachari, G. W. Trucks, J. A. Pople, M. Head-Gordon, A fifth-order perturbation comparison of electron correlation theories, *Chem. Phys. Lett.* 157 (1989) 479–483. doi:10.1016/S0009-2614(89)87395-6.
- [39] A. Pietropolli Charmet, P. Stoppa, S. Giorgianni, J. Bloino, N. Tasinato, I. Carnimeo, M. Biczysko, C. Puzzarini, Accurate vibrational-rotational parameters and infrared intensities of 1-bromo-1-fluoroethene: a joint experimental analysis and ab initio study, *J. Phys. Chem. A* 121 (17) (2017) 3305–3317.
- [40] C. Puzzarini, Accurate molecular structures of small-and medium-sized molecules, *Int. J. Quantum Chem.* 116 (21) (2016) 1513–1519.
- [41] C. Puzzarini, V. Barone, Diving for accurate structures in the ocean of molecular systems with the help of spectroscopy and quantum chemistry, *Acc. Chem. Res.* 51 (2) (2018) 548–556.
- [42] A. Halkier, T. Helgaker, P. Jorgensen, W. Klopper, J. Olsen, Basis-set convergence of the energy in molecular Hartree–Fock calculations, *Chem. Phys. Lett.* 302 (1999) 437–446. doi:10.1016/S0009-2614(99)00179-7.
- [43] T. Helgaker, W. Klopper, H. Koch, J. Noga, Basis-set convergence of correlated calculations on water, *J. Chem. Phys.* 106 (1997) 9639–9646. doi:10.1063/1.473863.
- [44] T. H. Dunning, Gaussian basis sets for use in correlated molecular calculations. I. The atoms boron through neon and hydrogen, *J. Chem. Phys.* 90 (1989) 1007–1023. doi:10.1063/1.456153.
- [45] D. E. Woon, T. H. Dunning, Gaussian basis sets for use in correlated molecular calculations. V. Core-valence basis sets for boron through neon, *J. Chem. Phys.* 103 (1995) 4572–4585. doi:10.1063/1.470645.
- [46] D. A. Matthews, L. Cheng, M. E. Harding, F. Lipparini and S. Stopkowitz, T.-C. Jagau, P. G. Szalay, J. Gauss, J. F. Stanton, Coupled-cluster techniques for computational chemistry: The CFOUR program package, *J. Chem. Phys.* 152 (2020) 214108. doi:10.1063/5.000483.
- [47] J. Gauss, J. F. Stanton, Analytic CCSD(T) second derivatives, *Chem. Phys. Lett.* 276 (1997) 70–77. doi:10.1016/S0009-2614(97)88036-0.
- [48] A. Pietropolli-Charmet, Y. Cornaton, Benchmarking fully analytic DFT force fields for vibrational spectroscopy: A study on halogenated compounds, *J. Mol. Struct.* 1160 (2018) 455–462. doi:10.1016/j.molstruc.2018.01.089.
- [49] D. Papoušek, M. R. Aliev, *Molecular vibrational-rotational spectra*, Elsevier, 1982.
- [50] M. R. Aliev, J. K. G. Watson, in: K. N. Rao (Ed.), *Molecular Spectroscopy: Modern Research*, Vol. III, Academic Press, New York, 1985, pp. 1–67.
- [51] J. K. G. Watson, Higher order *l*-doubling of linear molecules, *J. Mol. Spectrosc.* 101 (1983) 83.
- [52] I. E. Gordon, L. S. Rothman, R. J. Hargreaves, R. Hashemi, E. V. Karlovets, et al., The HITRAN2020 molecular spectroscopic database, *J. Quant. Spectrosc. Ra.* (2021) 107949doi:10.1016/j.jqsrt.2021.107949.
- [53] A. Jolly, Y. Benilan, A. Fayt, New infrared integrated band intensities for HC₃N and extensive line list for the ν_5 and ν_6 bending modes, *J. Mol. Spectrosc.* 242 (2007) 46–54. doi:10.1016/j.jms.2007.01.008.
- [54] A. Fayt, C. Vigouroux, F. Winther, Analysis of the ν_9 band complex of dicyanoacetylene and application of a theory of relative intensities to all subbands, *J. Mol. Spectrosc.* 224 (2) (2004) 114–130. doi:10.1016/j.jms.2004.01.004.
- [55] R. L. DeLeon, J. S. Muentner, Molecular beam electric resonance study of the ground and excited states of cyanoacetylene, *J. Chem. Phys.* 82 (1985) 1702–1704. doi:10.1063/1.448402.
- [56] I. E. Gordon, L. S. Rothman, C. Hill, R. V. Kochanov, Y. Tan, P. F. Bernath, M. Birk, V. Boudon, A. Campargue, K. Chance, et al., The HITRAN2016 molecular spectroscopic database, *J. Quant. Spectrosc. Ra.* 203 (2017) 3–69.
- [57] G. L. Villanueva, K. Magee-Sauer, M. J. Mumma, Modeling of nitrogen compounds in cometary atmospheres: Fluorescence models of ammonia (NH₃), hydrogen cyanide (HCN), hydrogen isocyanide (HNC) and cyanoacetylene (HC₃N), *J. Quant.*

- 552 Spectrosc. Ra. 129 (2013) 158–168. doi:10.1016/j.jqsrt.2013.06.010.
- 553 [58] E. Tiesinga, P. J. Mohr, D. B. Newell, B. N. Taylor, Codata recommended values of the fundamental physical constants:
554 2018, Rev. Mod. Phys. 93 (2021) 025010(1)–025010(63). doi:10.1103/RevModPhys.93.025010.
- 555 [59] R. El Hachtouki, J. Vander Auwera, Absolute line intensities in acetylene: The 1.5- μm region, J. Mol. Spectrosc. 216
556 (2002) 355–352. doi:0.1006/jmsp.2002.8660.
- 557 [60] A. Hansson, J. K. G. Watson, A comment on Hönl-London factors, J. Mol. Spectrosc. 233 (2005) 169–173.
- 558 [61] J. M. Brown, A. Carrington, Rotational Spectroscopy of Diatomic Molecules, Cambridge University Press, 2003.
- 559 [62] G. Wagner, B. P. Winnewisser, M. Winnewisser, K. Sarka, The Infrared-Spectrum of HC^{15}NO in the Range 170–1300
560 cm^{-1} , J. Mol. Spectrosc. 162 (1993) 82.
- 561 [63] M. Khlifi, F. Raulin, E. Arie, G. Graner, Absolute intensity of the IR bands of propynenitrile, J. Mol. Spectrosc. 143
562 (1990) 209–211. doi:10.1016/0022-2852(91)90085-0.
- 563 [64] M. Uyemura, S. Maeda, The infrared intensities of stretching fundamentals in gaseous and crystalline cyanoacetylene,
564 Bull. Chem. Soc. Japan 47 (1974) 2930–2935. doi:10.1246/bcsj.47.2930.